Three-dimensional culture modelling reveals divergent *Mycobacterium tuberculosis* virulence and antimicrobial treatment response

Magdalena K. Bielecka[1], Liku B.Tezera[1], Elena Konstantinopoulou[1], Nicola Casali[2], Orestis L. Katsamenis[3], Ximena Gonzalo[2], Francis Drobniewski[2] and Paul T. Elkington[1]

[1]NIHR Biomedical Research Centre, Clinical and Experimental Sciences Academic Unit, Faculty of Medicine, University of Southampton, UK. [2]Department of Infectious Disease, Imperial College London, UK. [3]µ-VIS X-ray Imaging Centre, Faculty of Engineering and Physical Sciences, University of Southampton, UK.

*** Correspondence:**

Paul T. Elkington

Clinical and Experimental Sciences

University of Southampton

Southampton SO16 1YD

UK

Tel: 00 44 23 8079 6671

E-mail: p.elkington@soton.ac.uk

Keywords: tuberculosis, mycobacteria, antimicrobial resistance, bioengineering, extracellular matrix, 3-dimensional cell culture

Running title: Mtb virulence in 3-D

Abstract

Tuberculosis (TB) remains a persistent epidemic, and the emergence of drug-resistant *Mycobacterium tuberculosis* (Mtb) presents a global healthcare threat. Whilst some new agents have been successfully introduced, innovative technologies to evaluate emerging anti-TB compounds are required to inform transformative approaches. Mtb is an obligate human pathogen, and consequently utilizing models that are consistent with human disease is likely to be critical. We have developed a human 3-dimensional (3-D) cell culture model that reflects human disease gene expression patterns and causes Mtb to become pyrazinamide sensitive *in vitro*. Here, we identify key differences in virulence between the standard laboratory strain, Mtb H37Rv, and clinical isolates. We demonstrate that Mtb H37Rv is attenuated in the 3-D system, more susceptible to antibiotics and hyper-inflammatory compared to clinical isolates. Prolonged *in vitro* culture of a clinical strain leads to attenuation. We then characterise antibiotic sensitivity of multi-drug-resistant Mtb within the 3-D model and define relative bactericidal activity. Finally, we demonstrate that verapamil increases efficacy of bedaquiline and delamanid antibiotic therapy. Taken together, our findings suggest that studying virulent clinical strains in an advanced cell culture system is a powerful adjunct to established methodologies to evaluate new interventions for TB.

Introduction

Tuberculosis (TB) continues to be a global epidemic, killing approximately 1.5 million people annually, and unfortunately the COVID-19 pandemic is likely to significantly worsen TB control (1). Furthermore, *Mycobacterium tuberculosis* (Mtb), the causative bacterium, is becoming progressively more resistant to antibiotics (2). Standard treatment takes a minimum of 6 months, and MDR-TB patients often require longer treatment for 18 months, with extensive drug side effects (3). Consequently, there is a pressing need for shortening therapy and discovering new chemotherapeutics (4).

Mtb H37Rv is a standard laboratory reference strain, which is very widely used for experimental purposes around the world. However, it was last isolated from a patient in 1905 (5, 6) and has been repeatedly sub-cultured in broth culture since then. Consequently, H37Rv has been widely proposed to be attenuated compared to clinical strains (7, 8). Modern circulating Mtb strains have been classified into multiple lineages (9), and some, such as Lineage 2 Beijing isolates, have contributed to large outbreaks of TB globally (10, 11).

Standard TB treatment involves four antibiotics initially, rifampicin, isoniazid, pyrazinamide and ethambutol for two months, followed by rifampicin and isoniazid for four months. Treatment of drug resistant Mtb requires longer courses of antibiotics, typically for greater than 12 months, with second-line agents often having lesser killing efficacy or a worse side-effect profile, such as moxifloxacin, D-cycloserine, para-amino salicylic acid, linezolid and amikacin. The most recently approved agents are bedaquiline and delamanid (3, 12). Recent studies of shorter treatments have had variable results (13-15), demonstrating that innovative technologies and new methods to investigate mechanisms of novel antibiotics are needed to predict optimal combinations of antimicrobial agents.

Enhanced drug resistance can be due to upregulation of bacterial efflux pumps, either through mutation or increased activity (16-20). In the zebrafish model of *M. marinum* infection, multi-drug tolerance develops in replicating mycobacteria by a macrophage-induced efflux mechanism (21). Importantly, intra-macrophage residence of the bacteria contributed to the phenomenon. Efflux pump inhibitors such as verapamil reduced tolerance to antibiotics including isoniazid and rifampicin (22) and MDR strains developed macrophage-induced drug tolerance and utilized efflux pumps for intracellular growth. Consequently, the calcium-channel blocker verapamil has emerged as a potential adjunctive chemotherapy for TB (23-25).

In this study, we investigate pathogenicity and antibiotic sensitivity of Mtb H37Rv compared to clinical Mtb isolates in broth culture and a 3-D primary human cellular granuloma model of TB infection, where host gene expression reflects events in patients more closely than standard cell culture (26-28), and Mtb is pyrazinamide sensitive (29). We demonstrate significant differences between laboratory and clinical strains in the 3-D system. We then investigate MDR-TB, and emerging therapies and combination treatment, further demonstrating the potential of adjunctive verapamil to increase antibiotic efficacy against clinical isolates when tested in an advanced cell culture model.

Experimental procedures

Mycobacteria culturing and reagents

The reference strain *Mycobacterium tuberculosis* H37Rv originated from Prof. Friedland's laboratory (Imperial College London), originally from the Pasteur institute, and Erdman and CDC 1551 strains were a gift from Dr Rawkins at Public Health England, Porton Down, UK. We obtained drug-sensitive clinical isolates and MDR-TB from Prof. Drobniewski (Imperial

College London) (11). Bioluminescent bacteria were routinely cultured in Middlebrook 7H9 medium (BD Biosciences, Oxford) supplemented with 10% ADC enrichment (SLS), 0.2% glycerol and 0.02% Tween 80 with kanamycin (25µg/ml) at 37°C in an incubator with shaking at 200 rpm. The 2-year old culture of the Beijing strain, 0414B lux, was generated by continuously repeating weekly 200µl sub-culture into a freshly prepared 2ml broth for this period. Bacteria were cultured until optical density of 0.6 was reached, which is equivalent to about 1x 10^8 CFU/ml. Either spectrophotometer (WPA Biowave CO8000 cell density meter, UK) or luminometer (GloMax® 20/20 Single Tube Luminometer; Promega, UK; detecting luminescence) was used to observe mycobacterial proliferation in 7H9 media. Reagents in this study were mainly Sigma-Aldrich acquired apart from delamanid and bedaquiline, which were bought from Adooq Bioscience, and tariquidar, diltiazem, amlodipine and carbonyl cyanide m-chlorophenyl hydrazine (CCCP), which were obtained from Tocris.

Generating bio-luminescent mycobacteria by electroporation

Bio-luminescent mycobacteria were generated by electroporation of pMV306hsp+LuxG13 plasmid (Addgene # 26161), into *M. tuberculosis* H37Rv, Erdman, CDC1551, clinical isolates and MDR strains (Table S1) as previously described (30, 31). We used 7H11 agar plates with kanamycin (25µg/ml) to select the strains transformed with an integrating vector. Luminescence of five randomly picked colonies was recorded and the transformants were checked by PCR with oligonucleotides (Forward: 5'- AACCGTATTACCGCCTTTGA-3' and Reverse: 5'- TATCAGCCCGTACCAGCATT-3') amplifying the corresponding promoter and reporter gene.

Infection of human peripheral blood mononuclear cells

Ethical approval was provided by the National Research Ethics Service Committee South Central - Southampton A, ref. 13/SC/0043. The National Health Service Blood and Transplant, Southampton, UK supplied us with single-donor buffy coats, from which peripheral blood mononuclear cells (PBMCs) were isolated using density gradient centrifugation over Ficoll-Paque (GE Healthcare Life Sciences, UK). Host cells were then infected with luminescent mycobacteria at a multiplicity of infection (MOI) of 0.1. After overnight incubation at 37°C in 5% CO_2, the infected PBMCs were treated with Versene solution for 10 min and neutralised by HBSS without Ca/Mg (Gibco). The cells were detached by scraping, placed in 50ml falcon tubes, topped up with HBSS and spun at 320xg for 8 min at 4°C. The supernatant was then decanted and the remaining pellet was re-suspended in RPMI 1640 solution with added 10μg/ml of ampicillin, 2mM of glutamine, 25μg/ml of kanamycin and 10% of human AB serum (to form a complete RPMI medium).

Cell encapsulation to form 3-D culture microspheres

Microspheres were generated as previously described (26, 32, 33). In short, to obtain a 3-D culture, we re-suspended Mtb-infected host cells in complete RPMI medium and combined with alginate-collagen matrix at 1 x 10^6 cells per ml. Microspheres were obtained by introducing the sterile mix into the Electrostatic Bead Generator (Nisco, Zurich, Switzerland) as described previously (34). Next, we equally distributed microspheres into 2ml Eppendorfs, immersed them in 1ml of complete RPMI medium and kept at 37°C with 5% CO_2. Bacterial bio-luminescence was observed with a GloMax® 20/20 Luminometer. In order to carry out colony counts, Mtb was released from microspheres by dissolving in 55mM Sodium citrate / 10mM EDTA with 1% saponin in HBSS, pelleting at 10,000xg in a

Heraeus™ Pico™ microcentrifuge and plating onto 7H11 agar. Colony forming units were counted at three weeks.

Imaging by micro-focus X-ray Computed Tomography (µCT)

µCT imaging was performed on the Nikon Med-X micro-CT scanner, optimised for biomedically relevant low-contrast specimens. The equipment is supplied with a 130 kVp X-ray source and a 2 x 2k flat panel detector allowing to obtain images at ~3µm spatial resolution. Microspheres containing PBMCs infected with Mtb H37Rv were harvested at day 14 and prepared for imaging. Samples were fixed for 1 h at room temperature and then overnight at 4°C in 3% glutaraldehyde in 0.1M cacodylate buffer (pH: 7.4) with an osmolarity of 850 mOsm plus 2mM $CaCl_2$. Fixed samples were then washed with the 0.1M cacodylate buffer (pH: 7.4), and post-fixed with 2% osmium tetroxide in 0.1M cacodylate buffer (plus 2mM $CaCl_2$ and 2.3M sucrose). A sample was, then, treated with a single wash step using a distilled water prior to staining it with 2% uranyl acetate (aq). Samples were dehydrated through a series of ethanol submersion steps in 30%, 50%, 70%, 95%, 100% alcohol solutions. The final 100% ethanol step was carried out twice. Next, the samples were immersed in acetonitrile in order to facilitate the passage from ethanol to resin. Samples were kept overnight in a 50:50 acetonitrile/ TAAB resin mixture. The next day, a fresh resin was prepared and samples were incubated in it for further 6 h. Subsequently, the samples were moved to embedding capsules with fresh TAAB resin. This resin block was scanned with µCT. The 3-D stack generated had a voxel size of 2.7µm.

3-D image processing

On a specific Amira workstation, 3-D image segmentation and analysis were done using FEI Amira software (version 6.4.0). In addition to the Wacom Cintiq 22HD touch-screen monitor (resolution 1920x1080 pixels), the workstations include an Intel Xeon processor with 24 cores, 192 GB of RAM, and an Nvidia Quadro K4200 4GB graphics card. Manual segmentation of microspheres containing aggregates (red), PBMC aggregates (blue), and single PBMCs (yellow) was carried out on the 3-D dataset of the resin block containing microspheres. 3-D reconstruction of the highlighted areas occurred using the 'Generate Surface' feature of Amira software. A smoothing function was applied to all three different labels to reduce the staircase effect. To visualise the result as a 3-D representation of the manual segmentation, the 'Surface View' object was attached to the surface file.

Scanning Electron Microscopy (SEM)

Initial fixation and processing to the completion of ethanol drying was as above. The microspheres were inserted in a metal holder with a grid after the final step of ethanol. Prior to SEM imaging, the lid of the holder was shut and the entire holder put in an absolute ethanol-filled glass vial. In order to achieve critical point drying, the samples were dried with a Balzers CPD 030 drier. On a stub covered with two-sided tape, dried microspheres were sprayed with gold and palladium (Pd), two non-oxidising metals, utilizing the Polaron E5100 sputter coater. This study was conducted with a FEI Quanta 200 Scanning Electron Microscope for the acquisition of SEM images. Up to 30kV of power and 100,000x magnification are available with this system. Ten kilovolts of power were used for acquisitions.

Eukaryotic Cell Viability/Toxicity Assays

Microspheres were equally distributed into two 96-well plates and incubated at 37°C. At day 3 and 7, respectively, one plate was sacrificed for cell viability analysis. Promega's CellTiter-Glo 3-D Cell Viability Assay was performed following the manufacturer's specifications. Cellular necrosis in microspheres was measured using CytoTox-Glo Cytotoxicity Assay (Promega). The GloMax® Discover 96 well plate reader (Promega, UK) was used to monitor the luminescence. Additionally, cell toxicity was determined by measuring the release of lactate dehydrogenase (LDH) with a colorimetric activity assay (Roche, Burgess Hill, United Kingdom). The collected supernatants were stored at 4°C for up to 7 days prior to analysis.

Luminex analysis

Supernatants were collected at day 3 and store at -20°C. Samples were sterilized by filtration through a 0.22 mM Durapore membrane (Millipore) (35). We followed manufacturer's protocol to determine concentrations of cytokines (Life Technologies, UK) and MMPs (R and D Systems, UK) in the samples using a Bioplex 200 platform (Bio-Rad, Hemel Hempstead, United Kingdom). Cytokine concentrations were measured using the cytokine 35-plex human panel (Thermofisher Scientific, UK). Analyses of MMP concentrations were done by MMP fluorokine multianalyte profiling (R&D Systems, Abingdon, UK).

Statistical Analysis

All experiments were carried out on a minimum of two separate occasions from different donors as biological replicates and each time with a minimum of three technical replicates.

208 Graph Pad Prism was utilized to carry out statistical analyses. Either ordinary one-way or 2-
209 way ANOVA Tukey's multiple comparisons tests were used to compare groups.

210

211

212 # Results

213 **Differential growth of Mtb strains in Middlebrook 7H9 broth versus 3-D microspheres**

214 To study Mtb proliferation in the context of host cells and extracellular matrix, we generated
215 3-dimensional microspheres, which consisted of human primary peripheral blood
216 mononuclear cells, Mtb and collagen (type I) using bio-electrospray methodology as
217 previously described (26, 27, 32, 33, 36). Scanning electron microscopy demonstrated the
218 external symmetry of the spheres (Fig. 1A). We characterised cellular aggregation within
219 spheres by micro-computed tomography (μ-CT), which demonstrated multicellular
220 granuloma formation at day 7 (Fig. 1B, C and Supplemental Video 1).

221 To monitor Mtb growth in our 3-D system, we generated luminescent clinical isolates by
222 incorporating the Lux operon (Table S1) (30). Microsphere luminescence closely correlates
223 with colony counts, permitting longitudinal analysis of growth within microspheres (32).
224 First, we compared Mtb proliferation in Middlebrook 7H9 broth to growth within
225 microspheres. The standard laboratory strain, H37Rv, grew significantly more rapidly in
226 broth culture than the clinical isolates ($p<0.0001$) (Fig. 1D). In contrast, in the 3-D system,
227 H37Rv was significantly attenuated in comparison to clinical isolates, which proliferated
228 much more rapidly over time (Fig. 1E). A similar pattern was observed when H37Rv was
229 compared with two other reference Mtb strains, CDC1551 and Erdman (Fig. S1). We then
230 repeatedly sub-cultured one of the clinical isolates of Beijing origin, 0414B, continuously in
231 7H9 broth for two years. This prolonged *in vitro* culture attenuated growth rate in infected
232 host cells in the 3-D model, to a similar extent to H37Rv, relative to freshly defrosted and
233 cultured 0414B (Fig. 1F). Therefore, the standard laboratory strain, H37Rv, is attenuated
234 compared to clinical isolates when analysed in a 3-D primary human cell culture model.

235

Despite increased proliferation, the clinical strain is not cytotoxic and cytokine secretion is suppressed

Next, we investigated the effect of increased growth of the clinical isolate 0414B on host cells in the 3-D system relative to the laboratory strain H37Rv. Host cells infected with either Mtb strain survived better relative to uninfected PBMCs at day 3, analysed by two different readouts, likely due to infection upregulation of pro-survival growth factors (Fig. 2A, B). However, we did not observe these differences using the Cell Titer Glo 3-D cell viability assay at this time point (Fig. 2C). Comparing Mtb-infected cells, a significant increase in toxicity with the clinical strain was only observed using CytoTox-Glo cytotoxicity assay (Fig. 2A), not with the LDH assay or Cell Titer Glo 3-D cell viability assays at the 3-day time point (Fig. 2B and C). There were some differences observed at the 7 day time point, with the clinical strain causing greater toxicity as measured by LDH release (Fig. S2B). These differences likely result from the technical features of the assays used, with LDH released from dying cells and stable for 7 days, so this provides a slightly different measure of cell death to the CytoTox-Glo cytotoxicity assay and Cell Titer-Glo assay. Later time points did not reveal any significant differences between strains using the two luminescent cell viability assays (Fig. S2A and C).

We compared the immunological response elicited by each strain at day 3, profiling secretion of inflammatory mediators by Luminex array. Despite the significantly higher mycobacterial load, secretion of pro-inflammatory cytokines was reduced from 0414B-infected microspheres in comparison to the lab strain H37Rv (Fig. 3). Suppressed cytokine release included TH_1 cytokines, TH_2 cytokines and some chemokines (Fig. 3 and Fig. S3). The secretion of other analytes, such as IL-17A, IL-8, MCP-1 was upregulated by Mtb infection

equally in response to both strains, indicating that 0414B did not induce a global hypo-secretory state. Similarly, secretion of the proteases matrix-metalloproteinase-1 (MMP-1) and MMP-7 was equally upregulated by H37Rv and 0414B (Fig. 3 and Fig. S3).

Clinical isolates are less susceptible to antibiotics in the 3-D system

Having observed accelerated growth but reduced cytokine secretion for 0414B relative to H37Rv in the microsphere system, we investigated relative efficacy of antibiotics against each strain. Cell culture media around spheres were supplemented with standard first line antibiotics: rifampicin, isoniazid, and pyrazinamide at physiological concentrations (1g/ml, 0.25g/ml and 500g/ml, respectively), on day 1 (32). The three-dimensional system demonstrated inhibitory effects of all three antibiotics on H37Rv growth (Fig. 4A) as previously reported, with luminescence falling progressively to baseline (32). In contrast, after initial suppression, the clinical isolate 0414B regrew at day 12 despite incubation with rifampicin and isoniazid (Fig. 4D). Furthermore, pyrazinamide was much less effective against the clinical isolate relative to the laboratory strain, with complete killing of H37Rv compared to temporary retardation of growth of 0414B. We tested a second clinical isolate, 1292F (lineage 4, Ural origin) with the four first-line drugs and once more observed regrowth. Again, pyrazinamide was less effective (Table 1). Therefore, clinical isolates are relatively more resistant to first line antibiotics in the 3-D model compared to the laboratory strain H37Rv.

With the emergence of drug-resistant TB, novel and repurposed second-line antibiotics have become increasingly important (2). Therefore, we analysed amikacin, moxifloxacin, D-cycloserine and linezolid in the microsphere system. Moxifloxacin and linezolid (5µg/ml and

24μg/ml, respectively) completely inhibited the growth of all the drug-sensitive strains in the 3-D system (Fig. 4B, E, Table 1). Amikacin was also as effective (Fig. 4B, E and Table 1), except for the Ural strain, 1292F, where the bacterial killing was relatively reduced (Table 1). D-cycloserine was effective against H37Rv but minimally effective for the 0414B strain (Fig. 4E), but was efficacious against 1561Y and had intermediate activity against 1292F (Table 1). PAS (20μg/ml) had similar efficacy against all clinical isolates examined, partially inhibiting growth (Table 1).

Finally, we tested emerging antibiotics bedaquiline and pretomanid (PA-824). Bedaquiline effectively killed the laboratory strain H37Rv, but was significantly less efficacious against the 0414B strain even at 10μg/ml (Fig. 4C, F). PA-824 completely inhibited growth of all strains studied (Fig. 4C, F, Table 1). These studies further confirmed increased antibiotic resistance in clinical strains relative to H37Rv.

Effect of anti-TB drugs on MDR-TB growth in 3-D model

Next, we investigated the efficacy of these antibiotics against MDR-TB in the 3-D model. As a proof of principle, we selected two MDR-TB clinical isolates 1471A and 0940Y, both belonging to the Beijing sub-lineage (Table S1), which have previously been characterised phenotypically by standard assays and genotypically (11). Strain 1471A was resistant to rifampicin, isoniazid and ethambutol, and strain 0940Y was resistant to rifampicin, isoniazid and pyrazinamide based on standard individually validated liquid culture methodology. As expected, rifampicin, isoniazid and ethambutol had no effect on 1471A growth, and pyrazinamide had a moderate inhibitory effect (Fig. 5A). Again, the pyrazinamide efficacy was reduced relative to H37Rv in the 3-D model. Strain 0940Y was resistant to rifampicin, isoniazid and pyrazinamide, as anticipated. Unexpectedly, the strain also was resistant to

ethambutol in our system (Fig. 5D). Ethambutol is a bacteriostatic agent at the concentrations used, and this may reflect the difficulty of reliable microbiological assays for this drug.

From the second-line drugs investigated, only D-cycloserine at the lower concentration of 20μg/ml had no efficacy against the two strains in the 3-D system (Fig. 5B, E). Amikacin, moxifloxacin and linezolid completely inhibited bacterial growth of both strains (Fig. 5B, C, E, F; Table 1). PAS and PA-824 were similarly effective in bacterial killing as against the laboratory strain H37Rv and for both MDR strains (Fig. 5 C, F and Table 1). Bedaquiline (10μg/ml) had no effect inhibiting 1471A growth, while it moderately inhibited 0940Y growth (Fig. 5C, F).

Verapamil potentiates the effect of emerging antibiotics in the 3-D system

These data demonstrate inherent antibiotic resistance in all Mtb clinical strains relative to H37Rv, and confirm further additional resistance within the MDR strains, suggesting that efflux pumps may be contributing to resistance and highlighting the need to investigate adjunctive therapy to increase bactericidal activity (25). We focused on bedaquiline and delamanid, important new MDR-TB drugs approved and recommended for treatment (2). Delamanid is relatively understudied with a partially defined mechanism of action (37). In 7H9 broth, regrowth occurred after initial killing even at a relatively high concentrations of delamanid (10μg/ml) (Fig. 6A, B). In contrast, delamanid fully inhibited bacterial growth in the 3-D system (Fig. 6C, D), demonstrating greater efficacy in the microsphere system relative to standard broth. The high delamanid concentrations required suggested efflux pump activity contributed to antibiotic resistance, and so we investigated this further.

Verapamil, a Ca^{2+} channel blocker, potentiates the killing of mycobacteria with rifampicin, isoniazid (22-24) or bedaquiline (21, 38, 39). Consistent with these observations, we demonstrated that verapamil potentiated the effect of bedaquiline in the 3-D system in killing both laboratory and clinical strains (Fig. 7A, D). The effect was most marked for the clinical strain, changing a minor suppression of growth to rapid killing, and a similar effect was observed in 7H9 broth (Fig. S4A, B). Next, we investigated whether verapamil could also potentiate the effect of delamanid. Delamanid efficacy was augmented by verapamil in the 3-D system for the clinical isolate 0414B, preventing re-growth at late time points (Fig. 7B, C, E, F). In 7H9 broth, regrowth of both strains was delayed in the presence of verapamil together with delamanid, and this effect was greater for the clinical isolates (Fig. S4B, C, E, F).

Finally, we investigated whether other Ca^{2+} channel blockers and efflux pump inhibitors had a similar potentiating effect on delamanid as verapamil (Fig. S5A). In a host environment, verapamil is an inhibitor of broad-spectrum ABC transporter systems [e.g. P-glycoprotein (P-gp/ABCB1) also known as multidrug resistance protein 1 (MDR1)], and so we studied a P-gp specific, third-generation inhibitor, tariquidar, which is also known to inhibit Breast Cancer Resistance Protein (BCRP/ABCG2) (40). Tariquidar did not potentiate the effect of delamanid (0.5μg/ml) at concentrations ranging 0.5-50μg/ml (Fig. S5B). Similarly, diltiazem, a non-dihydropyridine (DHP) member of the calcium channel blocker class, had no effect (Fig. S5C), while amlodipine, which is a dihydropyridine (DHP) calcium channel blocker, had very minor potentiating effect on delamanid at 30μg/ml (Fig. S5D). Additionally, we investigated two compounds that act not only at the host level but also directly on mycobacteria. Chlorpromazine, a type II NADH dehydrogenase (NDH-2) inhibitor (41) affecting Mtb oxidative phosphorylation, had only minimal potentiating effect

359 and carbonyl cyanide m-chlorophenyl hydrazine (CCCP), a proton uncoupler (42, 43), had no
360 potentiating effect at the concentrations tested (Fig. S5E, F). Overall, none of the compounds
361 investigated exhibited a potentiating effect on delamanid that was as potent at that of
362 verapamil, suggesting verapamil has a unique mode of action in increasing antibiotic efficacy
363 in relation to bacteria interacting with cells of a host.

Discussion

Tuberculosis remains a depressingly persistent global pandemic, and drug resistance is an increasing problem (2). Consequently, novel systems to evaluate antibiotic agents are needed to identify alternative treatment approaches and combinations. Previously, the typical route of identifying novel antibiotics was through the "three M's" route: minimal inhibitory concentration (MIC), mouse and man (44), centred on enriched liquid culture media for MIC and then minimum bactericidal activity (MBC) determination. Other more complex assays are less frequently employed to identify lead compounds. Although the "3M" approach is simple and straightforward, it does not incorporate the different physiological and anatomical microenvironments of granulomas and cavities in a patient's lung (45, 46), and the effect of these on drug penetration and activity. Consequently, this approach limits selection to compounds that are most effective against rapidly replicating bacteria, potentially omitting antibiotics that work against slowly replicating/dormant Mtb or are only efficacious in the context of a combined drug-host immune response. However, the more complex the assays, the more difficult, costly and lower the throughput for testing new compounds. In considering the cost of clinical trials, there is significant scope to increase the initial screening costs to save future expense; for example, a phase 3 novel antibiotic studies for hospital–acquired bacterial pneumonia cost $89,600 per patient enrolled (47).

Consequently, better *in vitro* systems are required for TB drug discovery (48, 49). This problem is illustrated by pyrazinamide, which would not have been identified through a traditional strategy; PZA is not bactericidal under standard culture conditions and works optimally under hypoxic conditions at pH 5.5 (50). Likewise, linezolid is bacteriostatic in standard culture media, but a potent agent as part of combination treatment for M/XDR-TB (2). The community is moving towards the concept of evaluating new combinations rather than evaluation of single agent. The results of the STREAM 1 trial support this,

389 demonstrating that a short regimen (9-11 months) was non-inferior to a long regimen with
390 respect to the primary efficacy outcome and has a similar safety profile (15). We need to
391 evaluate novel drugs, and drug combinations, using different early stage models that can
392 identify agents that complement each other in their ability to penetrate the range of TB
393 lesions and to kill all bacterial sub-populations inside them (44). In addition, the bacterial
394 strains evaluated need to be standardised for reproducibility, and include clinically relevant
395 ones.

396 Mtb H37Rv has been a mainstay in TB research, but was isolated from a patient in the
397 beginning of 20th century and has been repeatedly sub-cultured since (51, 52). Here, our 3-D
398 granuloma model shows that relative to the standard laboratory H37Rv strain, the clinical
399 strain 0414B is more virulent, hypo-inflammatory and inherently antibiotic resistant. The co-
400 administration of verapamil increases the efficacy of bedaquiline and delamanid, and this
401 effect is most pronounced for clinical strains. Our findings further highlight the importance
402 of including diverse strains in drug discovery studies (7, 8, 52, 53), whilst supporting the
403 utility of advanced cell culture models incorporating human cells to refine the drug discovery
404 pipeline (48, 54).

405 Mtb strains H37Rv and 0414B belong to Mtb lineages 4 and 2, respectively. In Middlebrook
406 7H9 broth, H37Rv grew much better than other strains investigated belonging to lineages 2
407 ('modern' Beijing strains) and lineage 4 (reference strains: Erdman and CDC1551), which
408 has been observed previously (55), but conversely was significantly attenuated in the
409 microspheres system compared to these strains. In experiments with mice, lineage 2 strains
410 produced high levels of bacilli in their lungs (56). Furthermore, studies using 2-D human cell
411 culture systems demonstrated that mycobacteria of this genotype replicate more rapidly in
412 comparison to the laboratory reference strains (57-59), and that lineage 2 strains spread more

413 rapidly between cells than H37Rv (60), supporting our observation of increased
414 pathogenicity.

415 Increased proliferation of the clinical strain was not associated with greater host cytotoxicity,
416 suggesting Mtb accumulates within host cells without destroying them. H37Rv was hyper-
417 inflammatory in contrast to the clinical isolates, inducing less cytokine secretion. Diverse
418 human and animal evidence suggests that the enhanced virulence of the Beijing strains is
419 partially due to induction of lower levels of Th1 cytokines such as TNF-α, IL-6, IL-10, IL-12
420 and IFN-γ (55, 58, 61-66). We did not observe any significant difference in the expression of
421 MCP-1 between the Beijing strain and laboratory strain, which has been shown previously
422 (61), and did not detect difference in the expression of IFN-α. It has been suggested that
423 Beijing strains induce more type 1 interferons (67, 68), however, other studies have shown
424 that IFN-α equalizes in lungs of BALB/c mice by day 14 (56), consistent with our findings.
425 Therefore, differences in the cytokine induction between strains clearly depends on the model
426 system studied.

427 We have previously shown that Mtb is pyrazinamide sensitive in the 3D model but not
428 standard 2-D culture (29). Here, antibiotic sensitivity testing in the 3-D model showed that
429 clinical isolates are significantly less susceptible to drugs than the laboratory strain, H37Rv.
430 Bedaquiline (10μg/ml) was ineffective against the 1471A strain and only slightly effective
431 for 0940Y clinical isolate, and bedaquiline resistance is emerging (69-72). This is likely due
432 to genotypical differences between the MDR strains. Sequencing of the strains investigated
433 revealed non-synonymous single nucleotide polymorphism (ns-SNP) differences in multiple
434 genes including efflux pumps and genes involved in respiration between the clinical isolates
435 and H37Rv (11). Whether this contributes to increased drug resistance of the clinical strains
436 needs to be determined (73-75). Evidently, the divergence between results from traditional
437 sensitivity testing methods and advanced cell culture systems has widespread clinical

implications, as *in vivo* Mtb is primarily within host phagocytes and under a stressed environment. For example, a synergistic effect between pyrazinamide and bedaquiline was recently highlighted by advanced imaging studies of infected human cells (50).

We investigated the response to emerging antibiotics bedaquiline and delamanid between the clinical isolate and the laboratory strain and explored the potential of verapamil in increasing efficacy. We observed that verapamil potentiates the killing effect of bedaquiline in our microsphere system, which has been previously reported in other models (25, 38, 39). We then showed that the effect of delamanid can similarly be potentiated by verapamil, although the effect was less marked. Verapamil augmentation for each antibiotic was greater for the clinical strain in the 3-D system, indicating strain-specific differences. Verapamil may result in a cascade of events involving the inhibition of respiratory chain complexes and energy production for efflux production in mycobacteria, and therefore the effect potentiating anti-TB drugs is indirectly increased (24). Verapamil's mechanism of action has been proposed to be through affecting the membrane energetics of *M. tuberculosis* (76) rather than a direct bacterial efflux pump inhibition as previously believed (23, 24, 38, 39), potentially explaining why other channel blockers were ineffective in our system. Overall, the potentiating effect of verapamil on the efficacy of antibiotics within the 3-D system was marked, in particular when clinical strains were studied.

Investigation of calcium channel blockers and efflux pump inhibitors other than verapamil had no combined effect with delamanid. Within our 3-D cell culture model, transport systems will be active on three separate membranes: the mycobacterial membrane, the phagolysosomal membrane and the macrophage cell membrane, representing a significant experimental challenge to fully dissect underlying mechanisms. At the same time, this reflects the true complexity of events in patients. We suspect that verapamil may be

462 enhancing the potency of delamanid by acting at all three membranes, and this additive effect
463 leads to the overall phenotype.

464 In conclusion, we demonstrate that clinical and laboratory strains have significantly different
465 virulence and antibiotic sensitivity when studied in a human 3-D cell culture system.
466 Prolonged subculture of a clinical strain leads to attenuation, demonstrating that the system
467 can be utilised to investigate mycobacterial pathogenic factors. Our data demonstrate that the
468 3-D bioelectrospray model, where gene expression reflects events in patients (27) and mirrors
469 the critical 3D granuloma organisation (46, 77), is an additional platform to test the
470 effectiveness of antibiotics and identifies differences in antibiotic sensitivity and the effect of
471 adjunctive therapy. Studying more complex assays at the preliminary drug development
472 stage may help identify and refine optimal lead combinations.

Conflict of interest: The authors declare that the research was conducted in the absence of any commercial or financial relationships that could be construed as a potential conflict of interest.

Author contributions: MK, LT and EK performed the laboratory analyses, NC and XG characterized the Mtb strains, OK supervised the micro-CT analyses, FD and PE conceived the project and coordinated the experiments. All authors had intellectual input into the progression of the project and contributed to the manuscript writing.

Funding: This work was supported by the UK Antimicrobial Resistance Cross Council Initiative funded by the Biotechnology and Biological Sciences Research Council and the Medical Research Council MR/N006631/1 and MR/P023754/1. We are grateful to NAMRIP (the Network for AntiMicrobial Resistance and Infection Prevention) for support, including pump-priming funding via NAMRIP's EPSRC grant NAMRA (EP/M027260/1), part of the EPSRC, Network for Antimicrobial Action, 'Bridging the Gap' programme. We thank the NIHR Imperial and Southampton BRCs for support.

Acknowledgements: We would like to thank Drs Jennifer Russell and Regina Teo, University of Southampton, for excellent technical assistance. We thank Dr Anton Page, Head of Biomedical Imaging Unit (BIU), University of Southampton, for providing support with electron scanning microscopy.

	Strain / Abx (µg/ml)	RIF 1	INH 0.25	PZA 500	EMB 4	AMIK 15	MOXI 5	DCS 20	LNZ 24	BDQ 10	PAS 20	PA-824 3
Lab Sensitive	H37Rv lux	+	+	+	+	+	+	+	+	+	+/-	+
	1292F lux	+	+	+/-	+	+/-	+	-/+	+	+	+/-	+
	1561Y lux	+	+	+/-	+	+	+	+	+	+/-	+/-	+
	0414B lux	+	+	-/+	+	+	+	-	+	-/+	+/-	+
MDR	1471A lux	-	-	-/+	-	+	+	-	+	-	+/-	+
	0940Y lux	-	-	-	-	+	+	-	+	-/+	+/-	+

Table 1: Summary of efficacy of antibiotics against different clinical isolates in the 3-D model. RIF - rifampicin; INH - isoniazid; PZA - pyrazinamide; EMB - ethambutol; AMIK - amikacin; MOXI - moxifloxacin; DCS - D-cycloserine; LNZ - linezolid; BDQ - bedaquiline; PAS - para-aminosalicylic acid; PA-824 - pretomanid.

Figure legends

Fig. 1: Mycobacterial clinical isolates grow more rapidly in the 3-D microsphere model. (A) Scanning electron microscopy of microspheres to demonstrate appearance. **(B, C)** Micro-CT scan (μCT) of embedded microspheres with 3-D reconstruction. Spheres appear different sizes as different levels have been captured within the block. (B) External appearance and cut surface. (C) Saggital section. Representative microspheres were marked in red, showing equal distribution of PBMCs within microsphere (yellow). A cellular aggregate is visible in the centre sphere (blue). **(D)** H37Rv lux grows faster than clinical isolates (1561Y lux, 0414B lux) and MDR-TB strains (1471A lux, 0940Y lux) in Middlebrook 7H9 broth measured by optical density (OD) at 600nm. Experiments were performed in triplicate. **(E)** Conversely, H37Rv lux growth in the 3-D system is attenuated in comparison to clinical isolates measured by luminescence. **(F)** Beijing lineage clinical isolate 0414B lux becomes attenauated after continuous 2-year culturing in broth when studied in the microsphere system, growing at a similar rate to the lab strain H37Rv lux, in contrast to freshly defrosted 0414B lux strain. **(E, F)** Data are the mean ± SEM of an experiment performed in triplicate and are representative of two separate experiments. Statistics: 2way ANOVA Tukey's multiple comparisons test **(D,E,F)**; **** $p<0.0001$.

Fig. 2: Host cells infected with Mtb H37Rv or a clinical strain have similar survival despite differences in bacterial proliferation. After infection with H37Rv lux (black) or 0414B lux (red), cells survived better than uninfected cells (A, B). A minimal difference was observed in relative host cell toxicity betweeen strains measured by CytoTox-Glo cytotoxicity assay (A), but no significant differences were seen with LDH cytotoxicity assay (B) and Cell Titer-Glo 3-D cell viability assay (C) between strains at day 3. Data are mean +/- SEM of 3 separate experiments. Statistics: Ordinary one-way ANOVA with Tukey's multiple comparisons test **(A, B, C)**; **** $p<0.0001$, ** $p<0.01$, * $p<0.1$, ns $p>0.05$.

Fig. 3: The clinical Mtb strain is less pro-inflammatory than 0414B. A heatmap of differences in cytokine secretion by PBMCs within microspheres after infection either with the laboratory strain

H37Rv lux or the clinical isolate 0414B lux, measured at day 3 by Luminex array. Cytokine secretion was normalised to concentration of H37Rv-infected cells (data are presented as a percentage normalised to H37Rv lux strain). Secretion of thirteen analytes was significantly reduced for the clinical strain in contrast to the lab strain, despite greater bacterial proliferation. Other analytes, such as IL-17A, MCP-1, MMP-1 and MMP-7, were equally upregulated by Mtb infection. Control: Uninfected PBMCs within microspheres. Normalised data from two donors analysed in triplicate are presented.

Fig. 4: The 0414B clinical strain is antibiotic resistant relative to Mtb H37Rv. Antibiotics were added at day 1 to the 3-D system and Mtb growth measured with luminescence; Standard drugs: rifampicin (RIF, 1µg/ml, dark red), isoniazid (INH, 0.25µg/ml, navy blue) and pyrazinamide (PZA, 500µg/ml; dark green); second-line drugs: amikacin (AMIK, 15µg/ml, mint green), moxifloxacin (MOXI, 5µg/ml, light brown) and D-cycloserine (DCS, 20µg/ml, lilac); emerging drugs: bedaquiline (BDQ, 10µg/ml, dark brown) and pretomanid (PA-824, 3µg/ml, light blue). H37Rv lux growth was inhibited by all antibiotics tested (A, B and C). The clinical isolate 0414B regrew at day 12 despite incubation with RIF and INH, and PZA was much less effective against the clinical isolate relative to the laboratory strain (D). From the second-line antibiotics, amikacin and moxifloxacin completely inhibited the clinical isolate's growth but D-cycloserine had only a minor effect (E). Similarly, bedaquiline had only a partial effect in contrast to PA-824, which was very effective against 0414B lux (F). Dimethyl sulfoxide (DMSO); used as solvent for rifampicin, bedaquiline and pretomanid in the control sample did not affect the growth of Mtb. Background level of luminescence is designated by crosses (x). Black arrow specifies antibitotic addition. The experiment was performed in triplicate on two separate donors, and a representative experiment is shown. Statistical analyses were done using 2way ANOVA Tukey's multiple comparisons test; **** $p<0.0001$. The data are very consistent, so SEM bars are very narrow and obscured.

Fig. 5: Multi-drug resistant (MDR) strains demonstrate extensive antibiotic resistance. Antibiotics were added at day 1 to the 3-D model and Mtb growth measured with luminescence; first-line drugs: rifampicin at 1µg/ml (RIF 1, dark red), isoniazid at 0.25µg/ml (INH 0.25, navy blue),

pyrazinamide at 500µg/ml (PZA 500, dark green) and ethambutol at 4µg/ml (EMB 4, orange); second-line drugs: moxifloxacin at 5µg/ml (MOXI 5, light brown), D-cycloserine at 20µg/ml (DCS 20, lilac) and 200µg/ml (DCS 200, dark purple) and linezolid at 24µg/ml (LNZ 24, mid-purple); emerging drugs: bedaquiline at 5µg/ml (BDQ 5, beige) and 10µg/ml (BDQ 10, dark brown); and pretomanid at 3µg/ml (PA-824 3, light blue). 1471A lux strain confirmed resistance to rifampicin, isoniazid and ethambutol and showed partial sensitivity to pyrazinamide (A). Growth of this multi-drug resistant clinical isolate was unaffected by the lower concentration of D-cycloserine and bedaquiline (both concentrations tested) (B, C). 0940Y lux strain was resistant to all first-line antibiotics (D) and D-cycloserine at the lower concentration (E). 0940Y had partial sensitivity to bedaquiline (F). Bacteria were fully inhibited by all other antibiotics examined. Mtb growth was unaltered by adding DMSO, used as solvent for rifampicin, linezolid, bedaquiline and PA-824. Crosses (x) designate background level of luminescence. Black arrow shows antibitotic addition. The experiment was performed in triplicate on two separate donors, and a representative experiment is shown. Statistical analyses were carried out using 2-way ANOVA with Tukey's multiple comparisons test; **** $p<0.0001$.

Fig. 6: Delamanid is more effective in microspheres than 7H9 broth. Delamanid was added at day 1 to either 7H9 broth (A, B) or infected microspheres (C, D) and Mtb growth monitored by luminescence. Bacteria were inhibited to the background level with delamanid at 10µg/ml (DLM 10, khaki green) in the microsphere system (C, D). Conversely, delamanid in 7H9 broth was much less effective in killing either H37Rv or O414B (A, B). Mtb growth was unaffected by DMSO, used as solvent for delamanid. Background level of luminescence is shown by crosses (x). Adding of antibiotics is marked by a black arrow. The experiment was performed in triplicate on two separate donors, and a representative experiment is shown. Statistical analyses were performed using 2-way ANOVA with Tukey's multiple comparisons test; **** $p<0.0001$, *** $p<0.001$.

Fig. 7: Verapamil increases efficacy of bedaqualine and delamanid in 3-D culture. Compounds were supplied at day 1 to the 3-D system and Mtb growth observed by luminescence; bedaquiline at 5µg/ml (BDQ 5, beige) and 10µg/ml (BDQ 10, dark brown); verapamil at 50µg/ml (VPL 50, light

blue); delamanid at 0.5µg/ml (DLM 0.5, orange) and 5µg/ml (DLM 5, light green). Verapamil alone slightly reduced the growth of Mtb in all conditions. Verapamil potentiated the effect of bedaquiline for both H37Rv lux and 0414B lux in the 3-D system (A, D). Delamanid at 0.5µg/ml combined with verapamil had a greater killing effect on the clinical isolate than on H37Rv (B, E). Delamanid at the higher concentration inhibited the bacterial growth to the background level (C, F). Slight re-growth was observed at a later time point for 0414B lux, which was inhibited when combined with verapamil. Mtb growth was unaffected by DMSO, used as solvent for all the compounds tested. Crosses (x) show background level of luminescence. Black arrow points to antibitotic addition. The experiment was performed in triplicate on two separate donors, and a representative experiment is shown. Statistics: 2way ANOVA Tukey's multiple comparisons test; **** $p<0.0001$, ** $p<0.01$, ns $p>0.05$

Supplementary materials

Fig. S1: Clinical isolate 0414B lux and other reference strains grow more rapidly in the 3-D model. (A) H37Rv lux grows faster than the clinical isolate 0414B lux and investigated reference strains (Erdman lux and CDC1551 lux) in Middlebrook 7H9 broth measured by optical density (OD) at 600nm. Experiments were performed in triplicate. **(B)** H37Rv lux is attenuated in comparison to the clinical isolate 0414B lux and the reference strains, Erdman lux and CDC1551 lux, in the 3-D system measured by luminescence. **(C)** Colony counts performed at day 26 confirm that H37Rv lux growth is reduced in comparison to the clinical isolate 0414B lux and the reference strains, Erdman lux and CDC1551 lux, in the 3-D system. Colour code as in (A) and (B). (B, C) Data are the mean ± the standard error of the mean of an experiment performed in triplicate and are representative of two separate experiments. Statistical analyses were carried out using 2-way ANOVA with Tukey's multiple comparisons test (A, B) or Ordinary one-way ANOVA Tukey's multiple comparisons test (C); **** $p<0.0001$, *** $p<0.001$, ** $p<0.01$.

Fig. S2: Survival of host cells at day 7. Upon infection with either H37Rv lux (black), reduced cytotoxity compared to uninfected cells was noted by LDH release and Cell Titer-Glo 3-D cell viability assay. When compared to 0414B lux (red), no difference was observed in host cell toxicity measured by CytoTox-Glo cytotoxicity assay (A) or Cell Titer-Glo 3-D cell viability assay (C) between strains. Toxicity of host cells infected with H37Rv lux was significantly lower than cells infected with clinical isolate 0414B lux at day 7 when analysed by the LDH cytotoxicity assay (B). Data are mean +/- SEM of 3 separate experiments. Statistics: Ordinary one-way ANOVA with Tukey's multiple comparisons test (A,B,C); *** $p<0.001$, * $p<0.1$, ns $p>0.05$.

Fig. S3: Secretion of multiple cytokines by 0414B-infected cells is reduced relative to H37Rv infected cells. The clinical isolate 0414B lux was significantly less pro-inflammatory than the laboratory strain H37Rv lux. Panels A, B, C, D, E and F show six significantly different cytokines in response to the two strains. Panels G, H, I, J, K and L illustrate cytokines and MMPs that were secretion was similary upregulated in response to the two strains, analysed in the same samples by Luminex multiplex array. Uninfected PBMCs are control. Normalised data from two donors

analysed in triplicate are presented (data are presented as a percentage vs H37Rv lux strain). Statistical analyses were performed using Ordinary one-way ANOVA with Tukey's multiple comparisons test; **** $p<0.0001$, *** $p<0.001$, ** $p<0.01$, * $p<0.1$, ns $p>0.05$.

Fig. S4: Verapamil increases Mtb killing in 7H9 broth. Anti-TB drugs were added at day 1 to 7H9 broth and Mtb growth monitored by luminescence; bedaquiline at 5µg/ml (BDQ 5, beige) and 10µg/ml (BDQ 10, dark brown); verapamil at 50µg/ml (VPL 50, light blue); delamanid at 0.5µg/ml (DLM 0.5, orange) and 5µg/ml (DLM 5, light green). Verapamil alone did not affect initial growth of Mtb, and had a minimal inhibitory effect at later time points (A, B, C, D, E, F). Bedaquiline was more effective against the clinical isolate than the laboratory strain (A, B). Verapamil's potentiating effect on bedaquiline in killing bacteria was observed at later time points for H37Rv lux (A) and minimally 0414B lux (B). Delamanid had substantial killing effect on Mtb, however bacteria quickly recovered (B, C, E, F). The decrease in bacterial growth was potentiated by verapamil and it was considerably greater for the clinical isolate relative to H37Rv, but bacteria revived at later time points (B, C, E, F). Mtb growth was unaffected by DMSO, used as solvent for all the compounds tested. Crosses (x) show background level of luminescence. Adding of antibiotics is specified by a black arrow. Data are mean +/- SEM for an experiment performed in triplicate and representative of 2 separate experiments. Statistical analyses were done using 2-way ANOVA with Tukey's multiple comparisons test; **** $p<0.0001$, * $p<0.1$, ns $p>0.05$.

Fig. S5: Alternative efflux pump inhibitors combined with delamanid do not have as potent an effect as verapamil in the 3-D system. Compounds were added at day 1 to 3-D culture and Mtb growth monitored by luminescence; delamanid at 0.5µg/ml (DLM 0.5, orange); verapamil at 50µg/ml (VPL 50, light blue); tariquidar at 0.5µg/ml (TQD 0.5, light grey-green), 5µg/ml (TQD 5, light brown), 10µg/ml (TQD 10, dark red) and 50µg/ml (TQD 50, dark brown); diltiazem at 5µg/ml (DLZ 5, light blue) and 50µg/ml (DLZ 50, mid-blue); amlodipine at 3µg/ml (AML 3, bright red) and 30µg/ml (AML 30, dark red); chlorpromazine at 2µg/ml (CPZ 2, light green) and 20µg/ml (CPZ 20, dark green); carbonyl cyanide 3-chlorophenylhydrazone at 2µg/ml (CCCP 2, lilac) and 20µg/ml (CCCP 20, mid-purple). Verapamil showed a potentiating effect on delamanid in inhibiting Mtb

growth (A). Addition of tariquidar, diltiazem or CCCP to delamanid had no effect at the concentrations tested (B, C, F). Supplementation of amlodipine with delamanid had minimal effect but only at a higher concentration used (D). Similarly, combining chlorpromazine 20µg/ml with delamanid showed very slight Mtb killing effect (E). Higher concentrations of tariquidar and chlorpromazine applied on their own (50µg/ml and 20µg/ml, respectively) had some inhibitory effect on the clinical isolate (B, E). Mtb growth was unaffected by DMSO, used as solvent for all the compounds tested. Crosses (x) represent background level of luminescence. Black arrow shows antibitotic addition. Data are mean +/- SEM for an experiment performed in triplicate and representative of 2 separate experiments. Statistical analyses were carried out using 2-way ANOVA with Tukey's multiple comparisons test; ns $p>0.05$

Supplementary video 1: Reconstruction of micro-CT images of Mtb-infected microspheres embedded in resin. For illustrative purposes, 3 microspheres have been highlighted, with cells within spheres highlighted yellow and cellular aggregates blue. Available for review at: https://www.dropbox.com/s/kcnooi7pj0xbibl/Microsphere_video_100719.mp4?dl=0

References:

1. Pai M, Kasaeva T, Swaminathan S. Covid-19's Devastating Effect on Tuberculosis Care - A Path to Recovery. N Engl J Med 2022; 386: 1490-1493. DOI: 10.1056/NEJMp2118145

2. Conradie F, Diacon AH, Ngubane N, Howell P, Everitt D, Crook AM, Mendel CM, Egizi E, Moreira J, Timm J, McHugh TD, Wills GH, Bateson A, Hunt R, Van Niekerk C, Li M, Olugbosi M, Spigelman M, Nix TBTT. Treatment of Highly Drug-Resistant Pulmonary Tuberculosis. N Engl J Med 2020; 382: 893-902. DOI: 10.1056/NEJMoa1901814

3. Dheda K, Barry CE, 3rd, Maartens G. Tuberculosis. Lancet 2016; 387: 1211-1226. DOI: 10.1016/S0140-6736(15)00151-8

4. Dartois VA, Rubin EJ. Anti-tuberculosis treatment strategies and drug development: challenges and priorities. Nat Rev Microbiol 2022 DOI: 10.1038/s41579-022-00731-y

5. Steenken W. Lysis of Tubercle Bacilli *in Vitro*. Experimental Biology and Medicine 1935; 33: 253-255. DOI: 10.3181/00379727-33-8330p

6. Kubica GPK, T. H.; Dunbar, F. P. . Designation of Strain H37Rv as the Neotype of *Mycobacterium tuberculosis*. International Journal of Systematic Bacteriology 1972; 22: 99-106. DOI: 10.1099/00207713-22-2-99

7. Andreu N, Gibert I. Cell population heterogeneity in *Mycobacterium tuberculosis* H37Rv. Tuberculosis (Edinb) 2008; 88: 553-559. DOI: 10.1016/j.tube.2008.03.005

8. Domenech P, Reed MB. Rapid and spontaneous loss of phthiocerol dimycocerosate (PDIM) from *Mycobacterium tuberculosis* grown in vitro: implications for virulence studies. Microbiology 2009; 155: 3532-3543. DOI: 10.1099/mic.0.029199-0

9. Brites D, Gagneux S. Co-evolution of Mycobacterium tuberculosis and Homo sapiens. Immunol Rev 2015; 264: 6-24. DOI: 10.1111/imr.12264

10. Merker M, Blin C, Mona S, Duforet-Frebourg N, Lecher S, Willery E, Blum MG, Rusch-Gerdes S, Mokrousov I, Aleksic E, Allix-Beguec C, Antierens A, Augustynowicz-Kopec E, Ballif M, Barletta F, Beck HP, Barry CE, 3rd, Bonnet M, Borroni E, Campos-Herrero I, Cirillo D, Cox H, Crowe S, Crudu V, Diel R, Drobniewski F, Fauville-Dufaux M, Gagneux S, Ghebremichael S, Hanekom M, Hoffner S, Jiao WW, Kalon S, Kohl TA, Kontsevaya I, Lillebaek T, Maeda S, Nikolayevskyy V, Rasmussen M, Rastogi N, Samper S, Sanchez-Padilla E, Savic B, Shamputa IC, Shen A, Sng LH, Stakenas P, Toit K, Varaine F, Vukovic D, Wahl C, Warren R, Supply P, Niemann S, Wirth T. Evolutionary history and global spread of the Mycobacterium tuberculosis Beijing lineage. Nat Genet 2015; 47: 242-249. DOI: 10.1038/ng.3195

11. Casali N, Nikolayevskyy V, Balabanova Y, Harris SR, Ignatyeva O, Kontsevaya I, Corander J, Bryant J, Parkhill J, Nejentsev S, Horstmann RD, Brown T, Drobniewski F. Evolution and transmission of drug-resistant tuberculosis in a Russian population. Nat Genet 2014; 46: 279-286. DOI: 10.1038/ng.2878

12. Khan PY, Franke MF, Hewison C, Seung KJ, Huerga H, Atwood S, Ahmed S, Khan M, Sultana T, Manzur-Ul-Alam M, Vo LNQ, Lecca L, Yae K, Kozhabekov S, Tamirat M, Gelin A, Vilbrun SC, Kikvidze M, Faqirzai J, Kadyrov A, Skrahina A, Mesic A, Avagyan N, Bastard M, Rich ML, Khan U, Mitnick CD. All-oral longer regimens are effective for the management of multidrug-resistant tuberculosis in high-burden settings. Eur Respir J 2022; 59 DOI: 10.1183/13993003.04345-2020

13. Warner DF, Mizrahi V. Shortening treatment for tuberculosis--to basics. N Engl J Med 2014; 371: 1642-1643. DOI: 10.1056/NEJMe1410977

14. Dorman SE, Nahid P, Kurbatova EV, Phillips PPJ, Bryant K, Dooley KE, Engle M, Goldberg SV, Phan HTT, Hakim J, Johnson JL, Lourens M, Martinson NA, Muzanyi G, Narunsky K, Nerette S, Nguyen NV, Pham TH, Pierre S, Purfield AE, Samaneka

W, Savic RM, Sanne I, Scott NA, Shenje J, Sizemore E, Vernon A, Waja Z, Weiner M, Swindells S, Chaisson RE, Group ACT, Tuberculosis Trials C. Four-Month Rifapentine Regimens with or without Moxifloxacin for Tuberculosis. N Engl J Med 2021; 384: 1705-1718. DOI: 10.1056/NEJMoa2033400

15. Nunn AJ, Phillips PPJ, Meredith SK, Chiang CY, Conradie F, Dalai D, van Deun A, Dat PT, Lan N, Master I, Mebrahtu T, Meressa D, Moodliar R, Ngubane N, Sanders K, Squire SB, Torrea G, Tsogt B, Rusen ID, Collaborators SS. A Trial of a Shorter Regimen for Rifampin-Resistant Tuberculosis. N Engl J Med 2019; 380: 1201-1213. DOI: 10.1056/NEJMoa1811867

16. De Rossi E, Ainsa JA, Riccardi G. Role of mycobacterial efflux transporters in drug resistance: an unresolved question. FEMS Microbiol Rev 2006; 30: 36-52. DOI: 10.1111/j.1574-6976.2005.00002.x

17. Louw GE, Warren RM, Gey van Pittius NC, Leon R, Jimenez A, Hernandez-Pando R, McEvoy CR, Grobbelaar M, Murray M, van Helden PD, Victor TC. Rifampicin reduces susceptibility to ofloxacin in rifampicin-resistant *Mycobacterium tuberculosis* through efflux. Am J Respir Crit Care Med 2011; 184: 269-276. DOI: 10.1164/rccm.201011-1924OC

18. Morris RP, Nguyen L, Gatfield J, Visconti K, Nguyen K, Schnappinger D, Ehrt S, Liu Y, Heifets L, Pieters J, Schoolnik G, Thompson CJ. Ancestral antibiotic resistance in *Mycobacterium tuberculosis*. Proc Natl Acad Sci U S A 2005; 102: 12200-12205. DOI: 10.1073/pnas.0505446102

19. Nguyen L, Thompson CJ. Foundations of antibiotic resistance in bacterial physiology: the mycobacterial paradigm. Trends Microbiol 2006; 14: 304-312. DOI: 10.1016/j.tim.2006.05.005

749 20. Piddock LJ. Multidrug-resistance efflux pumps - not just for resistance. Nat Rev
750 Microbiol 2006; 4: 629-636. DOI: 10.1038/nrmicro1464
751 21. Adams KN, Takaki K, Connolly LE, Wiedenhoft H, Winglee K, Humbert O, Edelstein
752 PH, Cosma CL, Ramakrishnan L. Drug tolerance in replicating mycobacteria
753 mediated by a macrophage-induced efflux mechanism. Cell 2011; 145: 39-53. DOI:
754 10.1016/j.cell.2011.02.022
755 22. Adams KN, Szumowski JD, Ramakrishnan L. Verapamil, and its metabolite
756 norverapamil, inhibit macrophage-induced, bacterial efflux pump-mediated tolerance
757 to multiple anti-tubercular drugs. J Infect Dis 2014; 210: 456-466. DOI:
758 10.1093/infdis/jiu095
759 23. Gupta S, Tyagi S, Almeida DV, Maiga MC, Ammerman NC, Bishai WR. Acceleration of
760 tuberculosis treatment by adjunctive therapy with verapamil as an efflux inhibitor.
761 Am J Respir Crit Care Med 2013; 188: 600-607. DOI: 10.1164/rccm.201304-0650OC
762 24. Machado D, Pires D, Perdigao J, Couto I, Portugal I, Martins M, Amaral L, Anes E,
763 Viveiros M. Ion Channel Blockers as Antimicrobial Agents, Efflux Inhibitors, and
764 Enhancers of Macrophage Killing Activity against Drug Resistant *Mycobacterium*
765 *tuberculosis*. PLoS One 2016; 11: e0149326. DOI: 10.1371/journal.pone.0149326
766 25. Ghajavand H, Kargarpour Kamakoli M, Khanipour S, Pourazar Dizaji S, Masoumi M,
767 Rahimi Jamnani F, Fateh A, Siadat SD, Vaziri F. High Prevalence of Bedaquiline
768 Resistance in Treatment-naive Tuberculosis Patients and Verapamil Effectiveness.
769 Antimicrob Agents Chemother 2019; 63 DOI: 10.1128/AAC.02530-18
770 26. Tezera LB, Bielecka MK, Chancellor A, Reichmann MT, Al Shammari B, Brace P, Batty
771 A, Tocheva A, Jogai S, Marshall BG, Tebruegge M, Jayasinghe SN, Mansour S,
772 Elkington PT. Dissection of the host-pathogen interaction in human tuberculosis using
773 a bioengineered 3-dimensional model. Elife 2017; 6 DOI: 10.7554/eLife.21283

774 27. Reichmann MT, Tezera LB, Vallejo AF, Vukmirovic M, Xiao R, Reynolds J, Jogai S,
775 Wilson S, Marshall B, Jones MG, Leslie A, D'Armiento JM, Kaminski N, Polak ME,
776 Elkington P. Integrated transcriptomic analysis of human tuberculosis granulomas and
777 a biomimetic model identifies therapeutic targets. J Clin Invest 2021; 131: e148136.
778 DOI: 10.1172/JCI148136
779 28. Elkington P, Polak ME, Reichmann MT, Leslie A. Understanding the tuberculosis
780 granuloma: the matrix revolutions. Trends Mol Med 2022; 28: 143-154. DOI:
781 10.1016/j.molmed.2021.11.004
782 29. Bielecka MK, Tezera LB, Zmijan R, Drobniewski F, Zhang X, Jayasinghe S, Elkington P.
783 A Bioengineered Three-Dimensional Cell Culture Platform Integrated with
784 Microfluidics To Address Antimicrobial Resistance in Tuberculosis. MBio 2017; 8:
785 e02073-02016. DOI: 10.1128/mBio.02073-16
786 30. Andreu N, Zelmer A, Fletcher T, Elkington PT, Ward TH, Ripoll J, Parish T, Bancroft
787 GJ, Schaible U, Robertson BD, Wiles S. Optimisation of bioluminescent reporters for
788 use with mycobacteria. PLoS One 2010; 5: e10777. DOI:
789 10.1371/journal.pone.0010777
790 31. Parish T, Stoker NG. Electroporation of mycobacteria. Methods Mol Biol 1998; 101:
791 129-144. DOI: 10.1385/0-89603-471-2:129
792 32. Bielecka MK, Tezera LB, Zmijan R, Drobniewski F, Zhang X, Jayasinghe S, Elkington P.
793 A Bioengineered Three-Dimensional Cell Culture Platform Integrated with
794 Microfluidics To Address Antimicrobial Resistance in Tuberculosis. MBio 2017; 8
795 DOI: 10.1128/mBio.02073-16
796 33. Tezera LB, Bielecka MK, Elkington PT. Bioelectrospray Methodology for Dissection of
797 the Host-pathogen Interaction in Human Tuberculosis. Bio Protoc 2017; 7 DOI:
798 10.21769/BioProtoc.2418

34. Workman VL, Tezera LB, Elkington PT, Jayasinghe SN. Controlled Generation of Microspheres Incorporating Extracellular Matrix Fibrils for Three-Dimensional Cell Culture. Adv Funct Mater 2014; 24: 2648-2657. DOI: 10.1002/adfm.201303891

35. Elkington PT, Green JA, Friedland JS. Filter sterilization of highly infectious samples to prevent false negative analysis of matrix metalloproteinase activity. J Immunol Methods 2006; 309: 115-119. DOI: 10.1016/j.jim.2005.11.010

36. Tezera LB, Bielecka MK, Ogongo P, Walker NF, Ellis M, Garay-Baquero DJ, Thomas K, Reichmann MT, Johnston DA, Wilkinson KA, Ahmed M, Jogai S, Jayasinghe SN, Wilkinson RJ, Mansour S, Thomas GJ, Ottensmeier CH, Leslie A, Elkington PT. Anti-PD-1 immunotherapy leads to tuberculosis reactivation via dysregulation of TNF-alpha. Elife 2020; 9 DOI: 10.7554/eLife.52668

37. Khoshnood S, Taki E, Sadeghifard N, Kaviar VH, Haddadi MH, Farshadzadeh Z, Kouhsari E, Goudarzi M, Heidary M. Mechanism of Action, Resistance, Synergism, and Clinical Implications of Delamanid Against Multidrug-Resistant Mycobacterium tuberculosis. Front Microbiol 2021; 12: 717045. DOI: 10.3389/fmicb.2021.717045

38. Gupta S, Cohen KA, Winglee K, Maiga M, Diarra B, Bishai WR. Efflux inhibition with verapamil potentiates bedaquiline in *Mycobacterium tuberculosis*. Antimicrob Agents Chemother 2014; 58: 574-576. DOI: 10.1128/AAC.01462-13

39. Gupta S, Tyagi S, Bishai WR. Verapamil increases the bactericidal activity of bedaquiline against *Mycobacterium tuberculosis* in a mouse model. Antimicrob Agents Chemother 2015; 59: 673-676. DOI: 10.1128/AAC.04019-14

40. Kannan P, Telu S, Shukla S, Ambudkar SV, Pike VW, Halldin C, Gottesman MM, Innis RB, Hall MD. The "specific" P-glycoprotein inhibitor Tariquidar is also a substrate and an inhibitor for breast cancer resistance protein (BCRP/ABCG2). ACS Chem Neurosci 2011; 2: 82-89. DOI: 10.1021/cn100078a

824 41. Weinstein EA, Yano T, Li LS, Avarbock D, Avarbock A, Helm D, McColm AA, Duncan
825 K, Lonsdale JT, Rubin H. Inhibitors of type II NADH:menaquinone oxidoreductase
826 represent a class of antitubercular drugs. Proc Natl Acad Sci U S A 2005; 102: 4548-
827 4553. DOI: 10.1073/pnas.0500469102
828 42. Heytler PG, Prichard WW. A new class of uncoupling agents--carbonyl cyanide
829 phenylhydrazones. Biochem Biophys Res Commun 1962; 7: 272-275. DOI:
830 43. Kasianowicz J, Benz R, McLaughlin S. The kinetic mechanism by which CCCP
831 (carbonyl cyanide m-chlorophenylhydrazone) transports protons across membranes. J
832 Membr Biol 1984; 82: 179-190. DOI:
833 44. Dartois V, Barry CE, 3rd. A medicinal chemists' guide to the unique difficulties of lead
834 optimization for tuberculosis. Bioorg Med Chem Lett 2013; 23: 4741-4750. DOI:
835 10.1016/j.bmcl.2013.07.006
836 45. Prideaux B, Via LE, Zimmerman MD, Eum S, Sarathy J, O'Brien P, Chen C, Kaya F,
837 Weiner DM, Chen PY, Song T, Lee M, Shim TS, Cho JS, Kim W, Cho SN, Olivier
838 KN, Barry CE, 3rd, Dartois V. The association between sterilizing activity and drug
839 distribution into tuberculosis lesions. Nat Med 2015; 21: 1223-1227. DOI:
840 10.1038/nm.3937
841 46. McCaffrey EF, Donato M, Keren L, Chen Z, Delmastro A, Fitzpatrick MB, Gupta S,
842 Greenwald NF, Baranski A, Graf W, Kumar R, Bosse M, Fullaway CC, Ramdial PK,
843 Forgo E, Jojic V, Van Valen D, Mehra S, Khader SA, Bendall SC, van de Rijn M,
844 Kalman D, Kaushal D, Hunter RL, Banaei N, Steyn AJC, Khatri P, Angelo M. The
845 immunoregulatory landscape of human tuberculosis granulomas. Nat Immunol 2022
846 DOI: 10.1038/s41590-021-01121-x
847 47. Stergiopoulos S, Calvert SB, Brown CA, Awatin J, Tenaerts P, Holland TL, DiMasi JA,
848 Getz KA. Cost Drivers of a Hospital-Acquired Bacterial Pneumonia and Ventilator-

Associated Bacterial Pneumonia Phase 3 Clinical Trial. Clin Infect Dis 2018; 66: 72-80. DOI: 10.1093/cid/cix726

48. Bielecka MK, Elkington P. Advanced cellular systems to study tuberculosis treatment. Curr Opin Pharmacol 2018; 42: 16-21. DOI: 10.1016/j.coph.2018.06.005

49. Aldridge BB, Barros-Aguirre D, Barry CE, 3rd, Bates RH, Berthel SJ, Boshoff HI, Chibale K, Chu XJ, Cooper CB, Dartois V, Duncan K, Fotouhi N, Gusovsky F, Hipskind PA, Kempf DJ, Lelievre J, Lenaerts AJ, McNamara CW, Mizrahi V, Nathan C, Olsen DB, Parish T, Petrassi HM, Pym A, Rhee KY, Robertson GT, Rock JM, Rubin EJ, Russell B, Russell DG, Sacchettini JC, Schnappinger D, Schrimpf M, Upton AM, Warner P, Wyatt PG, Yuan Y. The Tuberculosis Drug Accelerator at year 10: what have we learned? Nat Med 2021; 27: 1333-1337. DOI: 10.1038/s41591-021-01442-2

50. Santucci P, Greenwood DJ, Fearns A, Chen K, Jiang H, Gutierrez MG. Intracellular localisation of Mycobacterium tuberculosis affects efficacy of the antibiotic pyrazinamide. Nat Commun 2021; 12: 3816. DOI: 10.1038/s41467-021-24127-3

51. Borrell S, Trauner A, Brites D, Rigouts L, Loiseau C, Coscolla M, Niemann S, De Jong B, Yeboah-Manu D, Kato-Maeda M, Feldmann J, Reinhard M, Beisel C, Gagneux S. Reference set of Mycobacterium tuberculosis clinical strains: A tool for research and product development. PLoS ONE 2019; 14: e0214088. DOI: 10.1371/journal.pone.0214088

52. Ioerger TR, Feng Y, Ganesula K, Chen X, Dobos KM, Fortune S, Jacobs WR, Jr., Mizrahi V, Parish T, Rubin E, Sassetti C, Sacchettini JC. Variation among genome sequences of H37Rv strains of *Mycobacterium tuberculosis* from multiple laboratories. J Bacteriol 2010; 192: 3645-3653. DOI: 10.1128/JB.00166-10

873 53. Molina-Torres CA, Castro-Garza J, Ocampo-Candiani J, Monot M, Cole ST, Vera-
874 Cabrera L. Effect of serial subculturing on the genetic composition and cytotoxic
875 activity of *Mycobacterium tuberculosis*. J Med Microbiol 2010; 59: 384-391. DOI:
876 10.1099/jmm.0.015966-0
877 54. Elkington P, Lerm M, Kapoor N, Mahon R, Pienaar E, Huh D, Kaushal D, Schlesinger
878 LS. In Vitro Granuloma Models of Tuberculosis: Potential and Challenges. J Infect
879 Dis 2019; 219: 1858-1866. DOI: 10.1093/infdis/jiz020
880 55. Sarkar R, Lenders L, Wilkinson KA, Wilkinson RJ, Nicol MP. Modern lineages of
881 *Mycobacterium tuberculosis* exhibit lineage-specific patterns of growth and cytokine
882 induction in human monocyte-derived macrophages. PLoS One 2012; 7: e43170.
883 DOI: 10.1371/journal.pone.0043170
884 56. Lopez B, Aguilar D, Orozco H, Burger M, Espitia C, Ritacco V, Barrera L, Kremer K,
885 Hernandez-Pando R, Huygen K, van Soolingen D. A marked difference in
886 pathogenesis and immune response induced by different *Mycobacterium tuberculosis*
887 genotypes. Clin Exp Immunol 2003; 133: 30-37. DOI:
888 57. Li Q, Whalen CC, Albert JM, Larkin R, Zukowski L, Cave MD, Silver RF. Differences in
889 Rate and Variability of Intracellular Growth of a Panel of *Mycobacterium*
890 *tuberculosis* Clinical Isolates within a Human Monocyte Model. Infect Immun 2002;
891 70: 6489-6493. DOI: 10.1128/iai.70.11.6489-6493.2002
892 58. Theus SA, Cave MD, Eisenach KD. Intracellular macrophage growth rates and cytokine
893 profiles of *Mycobacterium tuberculosis* strains with different transmission dynamics.
894 J Infect Dis 2005; 191: 453-460. DOI: 10.1086/425936
895 59. Zhang M, Gong J, Yang Z, Samten B, Cave MD, Barnes PF. Enhanced capacity of a
896 widespread strain of *Mycobacterium tuberculosis* to grow in human macrophages. J
897 Infect Dis 1999; 179: 1213-1217. DOI: 10.1086/314738

60. Zha BS, Desvignes L, Fergus TJ, Cornelius A, Cheng TY, Moody DB, Ernst JD. Bacterial Strain-Dependent Dissociation of Cell Recruitment and Cell-to-Cell Spread in Early M. tuberculosis Infection. MBio 2022: e0133222. DOI: 10.1128/mbio.01332-22

61. Huet G, Constant P, Malaga W, Laneelle MA, Kremer K, van Soolingen D, Daffe M, Guilhot C. A lipid profile typifies the Beijing strains of *Mycobacterium tuberculosis*: identification of a mutation responsible for a modification of the structures of phthiocerol dimycocerosates and phenolic glycolipids. J Biol Chem 2009; 284: 27101-27113. DOI: 10.1074/jbc.M109.041939

62. Rakotosamimanana N, Raharimanga V, Andriamandimby SF, Soares JL, Doherty TM, Ratsitorahina M, Ramarokoto H, Zumla A, Huggett J, Rook G, Richard V, Gicquel B, Rasolofo-Razanamparany V, Group VVS. Variation in gamma interferon responses to different infecting strains of *Mycobacterium tuberculosis* in acid-fast bacillus smear-positive patients and household contacts in Antananarivo, Madagascar. Clin Vaccine Immunol 2010; 17: 1094-1103. DOI: 10.1128/CVI.00049-10

63. Reed MB, Domenech P, Manca C, Su H, Barczak AK, Kreiswirth BN, Kaplan G, Barry CE, 3rd. A glycolipid of hypervirulent tuberculosis strains that inhibits the innate immune response. Nature 2004; 431: 84-87. DOI: 10.1038/nature02837

64. Sohn H, Lee KS, Kim SY, Shin DM, Shin SJ, Jo EK, Park JK, Kim HJ. Induction of cell death in human macrophages by a highly virulent Korean Isolate of *Mycobacterium tuberculosis* and the virulent strain H37Rv. Scand J Immunol 2009; 69: 43-50. DOI: 10.1111/j.1365-3083.2008.02188.x

65. Tanveer M, Hasan Z, Kanji A, Hussain R, Hasan R. Reduced TNF-alpha and IFN-gamma responses to Central Asian strain 1 and Beijing isolates of *Mycobacterium*

922 *tuberculosis* in comparison with H37Rv strain. Trans R Soc Trop Med Hyg 2009;
923 103: 581-587. DOI: 10.1016/j.trstmh.2009.03.014
924 66. Wang C, Peyron P, Mestre O, Kaplan G, van Soolingen D, Gao Q, Gicquel B, Neyrolles
925 O. Innate immune response to *Mycobacterium tuberculosis* Beijing and other
926 genotypes. PLoS One 2010; 5: e13594. DOI: 10.1371/journal.pone.0013594
927 67. Manca C, Tsenova L, Bergtold A, Freeman S, Tovey M, Musser JM, Barry CE, 3rd,
928 Freedman VH, Kaplan G. Virulence of a *Mycobacterium tuberculosis* clinical isolate
929 in mice is determined by failure to induce Th1 type immunity and is associated with
930 induction of IFN-alpha /beta. Proc Natl Acad Sci U S A 2001; 98: 5752-5757. DOI:
931 10.1073/pnas.091096998
932 68. Manca C, Tsenova L, Freeman S, Barczak AK, Tovey M, Murray PJ, Barry C, Kaplan G.
933 Hypervirulent M. tuberculosis W/Beijing strains upregulate type I IFNs and increase
934 expression of negative regulators of the Jak-Stat pathway. J Interferon Cytokine Res
935 2005; 25: 694-701. DOI: 10.1089/jir.2005.25.694
936 69. Degiacomi G, Sammartino JC, Sinigiani V, Marra P, Urbani A, Pasca MR. In vitro Study
937 of Bedaquiline Resistance in Mycobacterium tuberculosis Multi-Drug Resistant
938 Clinical Isolates. Front Microbiol 2020; 11: 559469. DOI:
939 10.3389/fmicb.2020.559469
940 70. Ismail NA, Omar SV, Moultrie H, Bhyat Z, Conradie F, Enwerem M, Ferreira H, Hughes
941 J, Joseph L, Kock Y, Letsaolo V, Maartens G, Meintjes G, Ngcamu D, Okozi N,
942 Padanilam X, Reuter A, Romero R, Schaaf S, Te Riele J, Variava E, van der Meulen
943 M, Ismail F, Ndjeka N. Assessment of epidemiological and genetic characteristics and
944 clinical outcomes of resistance to bedaquiline in patients treated for rifampicin-
945 resistant tuberculosis: a cross-sectional and longitudinal study. Lancet Infect Dis 2021
946 DOI: 10.1016/S1473-3099(21)00470-9

947 71. Kaniga K, Hasan R, Jou R, Vasiliauskiene E, Chuchottaworn C, Ismail N, Metchock B,
948 Miliauskas S, Viet Nhung N, Rodrigues C, Shin S, Simsek H, Smithtikarn S, Ngoc
949 ALT, Boonyasopun J, Kazi M, Kim S, Kamolwat P, Musteikiene G, Sacopon CA,
950 Tahseen S, Vasiliauskaite L, Wu MH, Vally Omar S. Bedaquiline Drug Resistance
951 Emergence Assessment in Multidrug-Resistant Tuberculosis (MDR-TB): a 5-Year
952 Prospective In Vitro Surveillance Study of Bedaquiline and Other Second-Line Drug
953 Susceptibility Testing in MDR-TB Isolates. J Clin Microbiol 2022; 60: e0291920.
954 DOI: 10.1128/JCM.02919-20
955 72. Wu SH, Chan HH, Hsiao HC, Jou R. Primary Bedaquiline Resistance Among Cases of
956 Drug-Resistant Tuberculosis in Taiwan. Front Microbiol 2021; 12: 754249. DOI:
957 10.3389/fmicb.2021.754249
958 73. Andries K, Villellas C, Coeck N, Thys K, Gevers T, Vranckx L, Lounis N, de Jong BC,
959 Koul A. Acquired resistance of *Mycobacterium tuberculosis* to bedaquiline. PLoS
960 One 2014; 9: e102135. DOI: 10.1371/journal.pone.0102135
961 74. Kanji A, Hasan R, Ali A, Zaver A, Zhang Y, Imtiaz K, Shi W, Clark TG, McNerney R,
962 Phelan J, Rao S, Shafiq S, Hasan Z. Single nucleotide polymorphisms in efflux pumps
963 genes in extensively drug resistant *Mycobacterium tuberculosis* isolates from
964 Pakistan. Tuberculosis (Edinb) 2017; 107: 20-30. DOI: 10.1016/j.tube.2017.07.012
965 75. Liu J, Shi W, Zhang S, Hao X, Maslov DA, Shur KV, Bekker OB, Danilenko VN, Zhang
966 Y. Mutations in Efflux Pump Rv1258c (Tap) Cause Resistance to Pyrazinamide,
967 Isoniazid, and Streptomycin in *M. tuberculosis*. Front Microbiol 2019; 10: 216. DOI:
968 10.3389/fmicb.2019.00216
969 76. Chen C, Gardete S, Jansen RS, Shetty A, Dick T, Rhee KY, Dartois V. Verapamil Targets
970 Membrane Energetics in *Mycobacterium tuberculosis*. Antimicrob Agents Chemother
971 2018; 62 DOI: 10.1128/AAC.02107-17

77. Gideon HP, Hughes TK, Tzouanas CN, Wadsworth MH, 2nd, Tu AA, Gierahn TM, Peters JM, Hopkins FF, Wei JR, Kummerlowe C, Grant NL, Nargan K, Phuah JY, Borish HJ, Maiello P, White AG, Winchell CG, Nyquist SK, Ganchua SKC, Myers A, Patel KV, Ameel CL, Cochran CT, Ibrahim S, Tomko JA, Frye LJ, Rosenberg JM, Shih A, Chao M, Klein E, Scanga CA, Ordovas-Montanes J, Berger B, Mattila JT, Madansein R, Love JC, Lin PL, Leslie A, Behar SM, Bryson B, Flynn JL, Fortune SM, Shalek AK. Multimodal profiling of lung granulomas in macaques reveals cellular correlates of tuberculosis control. Immunity 2022; 55: 827-846 e810. DOI: 10.1016/j.immuni.2022.04.004

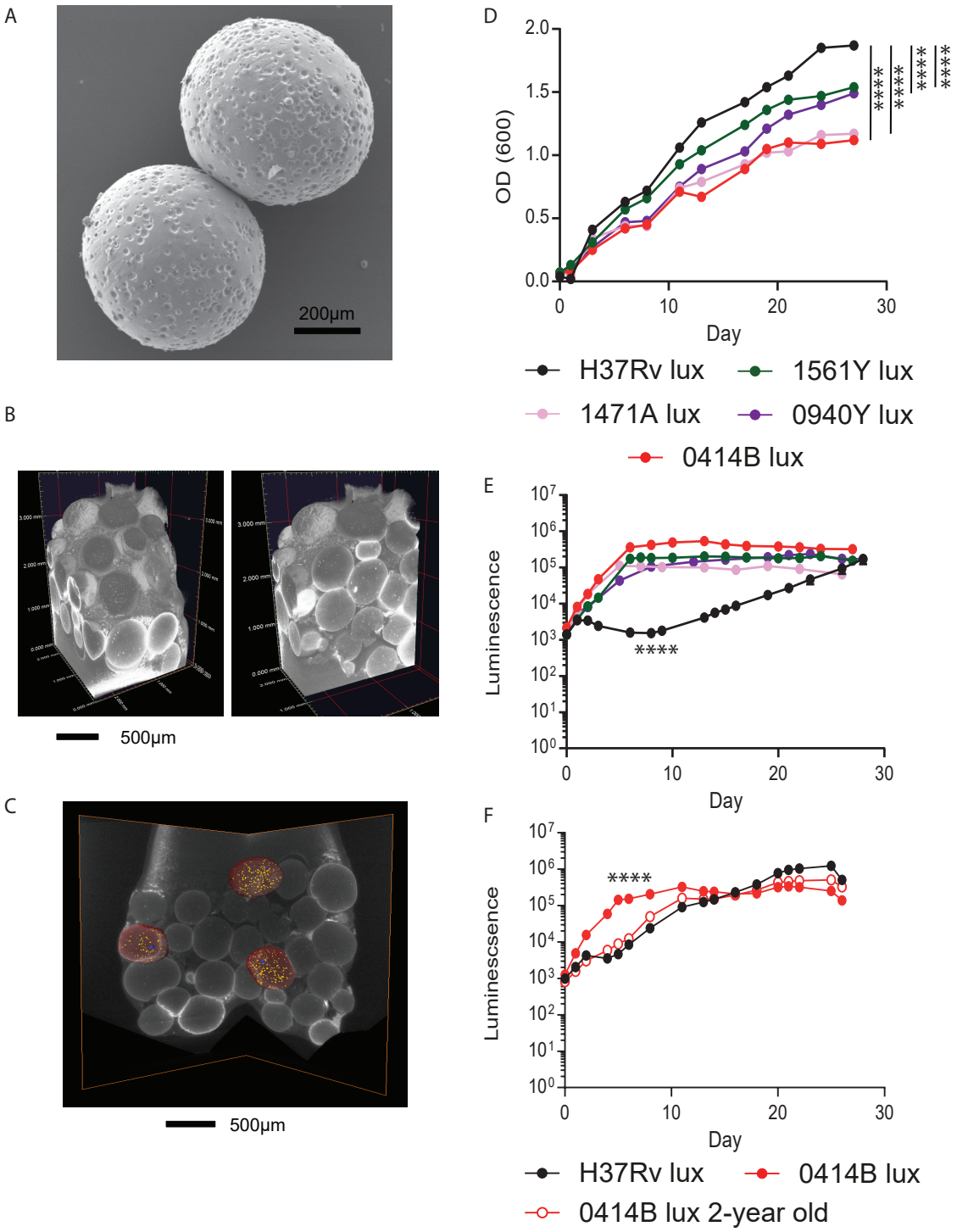

Fig. 1: Mycobacterial clinical isolates grow more rapidly in the 3-D microsphere model. (A) Scanning electron microscopy of microspheres to demonstrate appearance. **(B, C)** Micro-CT scan (µCT) of embedded microspheres with 3-D reconstruction. Spheres appear different sizes as different levels have been captured within the block. (B) External appearance and cut surface. (C) Saggital section. Representative microspheres were marked in red, showing equal distribution of PBMCs within microsphere (yellow). A cellular aggregate is visible in the centre sphere (blue). **(D)** H37Rv lux grows faster than clinical isolates (1561Y lux, 0414B lux) and MDR-TB strains (1471A lux, 0940Y lux) in Middlebrook 7H9 broth measured by optical density (OD) at 600nm. Experiments were performed in triplicate. **(E)** Conversely, H37Rv lux growth in the 3-D system is attenuated in comparison to clinical isolates measured by luminescence. **(F)** Beijing lineage clinical isolate 0414B lux becomes attenauated after continuous 2-year culturing in broth when studied in the microsphere system, growing at a similar rate to the lab strain H37Rv lux, in contrast to freshly defrosted 0414B lux strain. **(E, F)** Data are the mean ± SEM of an experiment performed in triplicate and are representative of two separate experiments. Statistics: 2way ANOVA Tukey's multiple comparisons test **(D,E,F)**; **** $p<0.0001$.

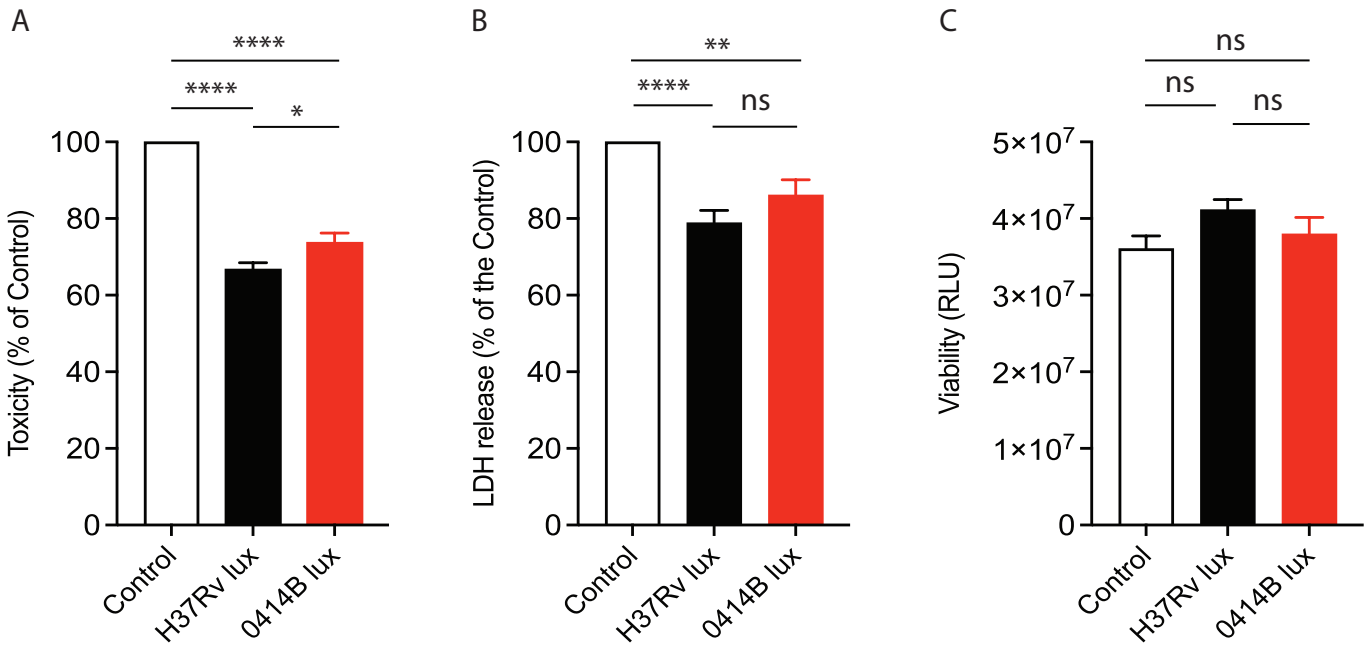

Fig. 2: Host cells infected with Mtb H37Rv or a clinical strain have similar survival despite differences in bacterial proliferation. After infection with H37Rv lux (black) or 0414B lux (red), cells survived better than uninfected cells (A, B). A minimal difference was observed in relative host cell toxicity betweeen strains measured by CytoTox-Glo cytotoxicity assay (A), but no significant differences were seen with LDH cytotoxicity assay (B) and Cell Titer-Glo 3-D cell viability assay (C) between strains at day 3. Data are mean +/- SEM of 3 separate experiments. Statistics: Ordinary one-way ANOVA with Tukey's multiple comparisons test **(A, B, C)**; **** $p<0.0001$, ** $p<0.01$, * $p<0.1$, ns $p>0.05$.

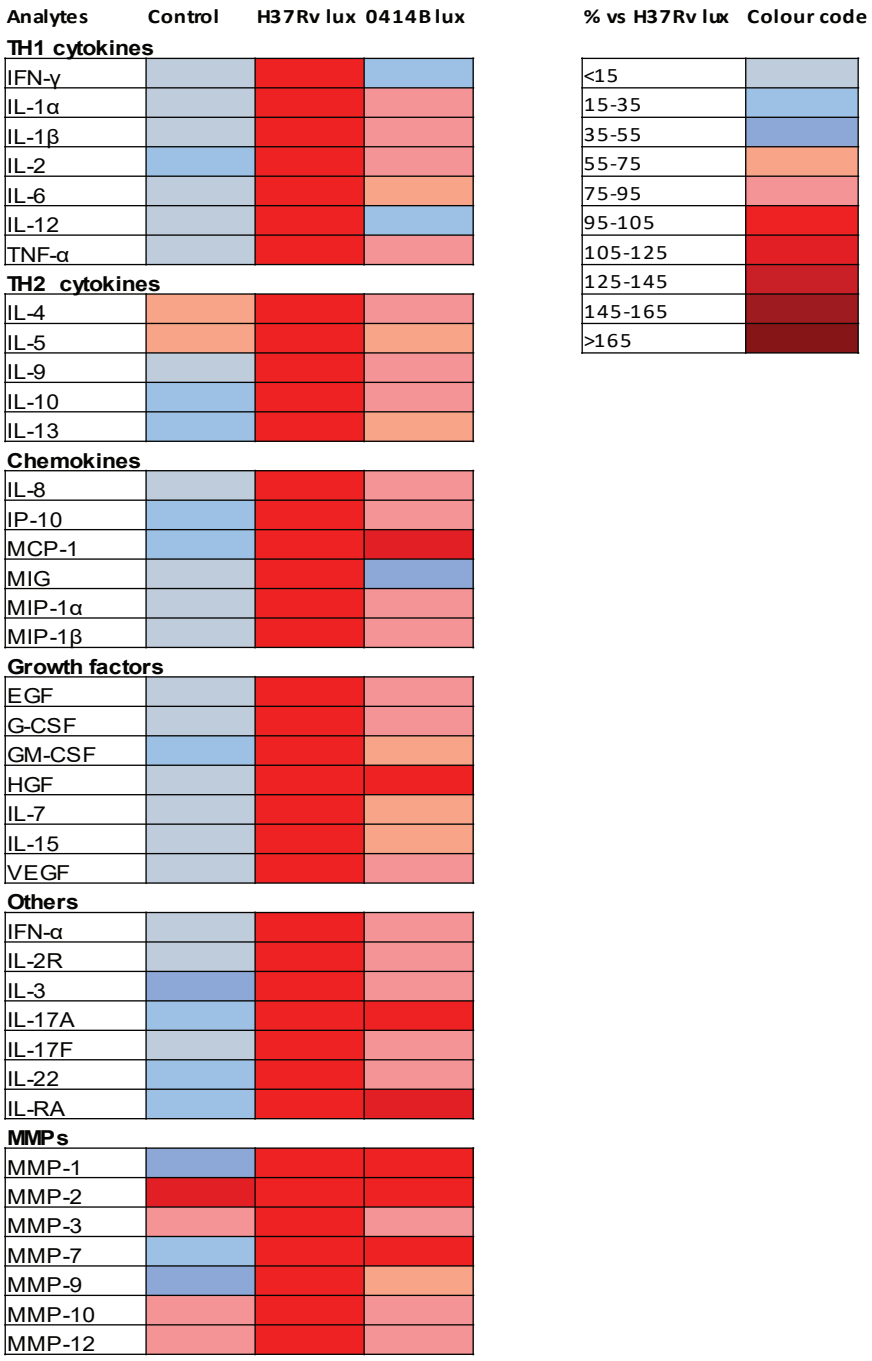

Fig. 3: The clinical Mtb strain is less pro-inflammatory than 0414B. A heatmap of differences in cytokine secretion by PBMCs within microspheres after infection either with the laboratory strain H37Rv lux or the clinical isolate 0414B lux, measured at day 3 by Luminex array. Cytokine secretion was normalised to concentration of H37Rv-infected cells (data are presented as a percentage normalised to H37Rv lux strain). Secretion of thirteen analytes was significantly reduced for the clinical strain in contrast to the lab strain, despite greater bacterial proliferation. Other analytes, such as IL-17A, MCP-1, MMP-1 and MMP-7, were equally upregulated by Mtb infection. Control: Uninfected PBMCs within microspheres. Normalised data from two donors analysed in triplicate are presented.

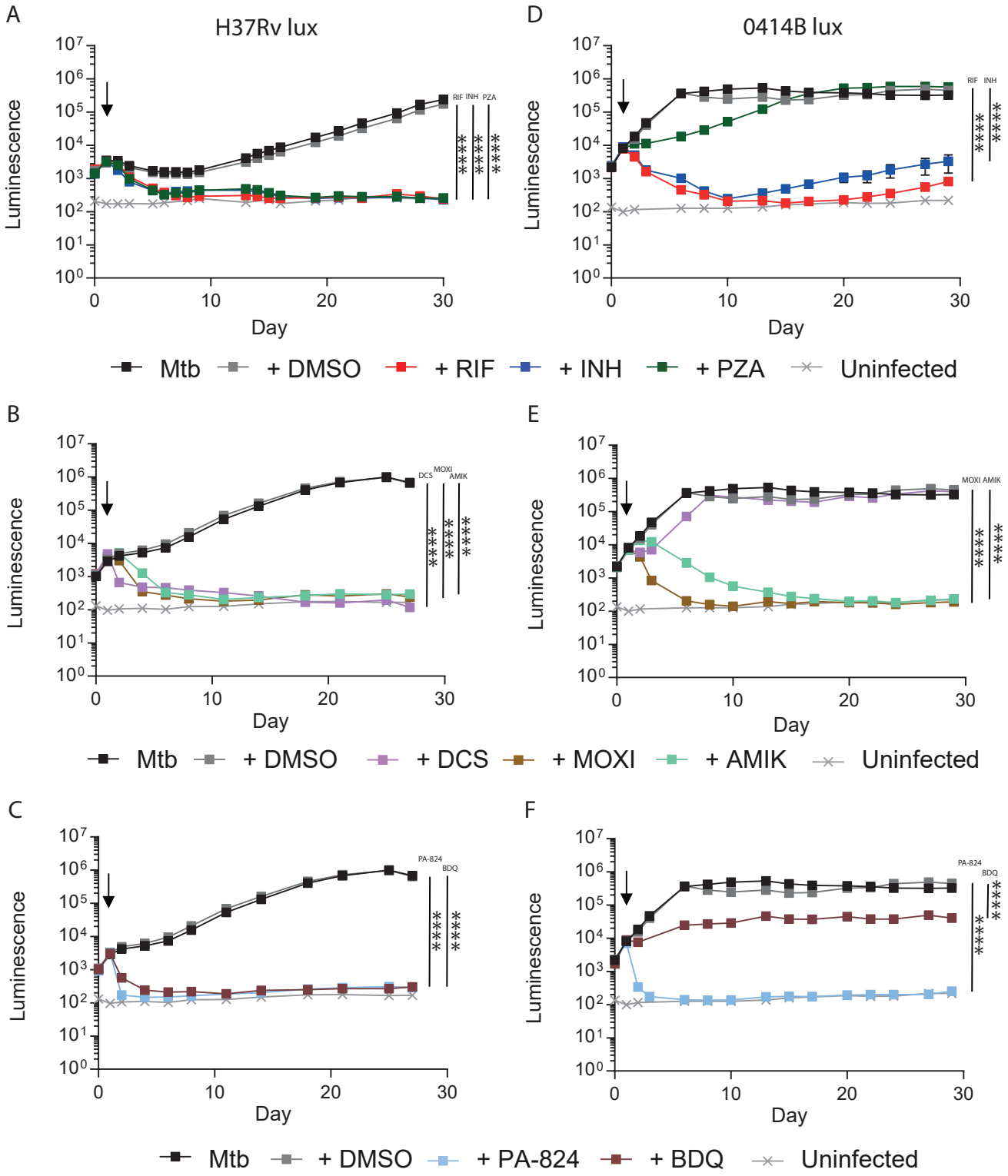

Fig. 4: The 0414B clinical strain is antibiotic resistant relative to Mtb H37Rv. Antibiotics were added at day 1 to the microsphere system and Mtb growth monitored by luminescence; Standard drugs: rifampicin (RIF, 1µg/ml, dark red), isoniazid (INH, 0.25µg/ml, navy blue) and pyrazinamide (PZA, 500µg/ml; dark green); second-line drugs: amikacin (AMIK, 15µg/ml, mint green), moxifloxacin (MOXI, 5µg/ml, light brown) and D-cycloserine (DCS, 20µg/ml, lilac); emerging drugs: bedaquiline (BDQ, 10µg/ml, dark brown) and pretomanid (PA-824, 3µg/ml, light blue). H37Rv lux growth was inhibited by all antibiotics tested (A, B and C). The clinical isolate 0414B regrew at day 12 despite incubation with RIF and INH, and PZA was much less effective against the clinical isolate relative to the laboratory strain (D). From the second-line antibiotics, amikacin and moxifloxacin completely inhibited the clinical isolate's growth but D-cycloserine had only a minor effect (E). Similarly, bedaquiline had only a partial effect in contrast to PA-824, which was very effective against 0414B lux (F). Mtb growth was unaffected in the control sample with dimethyl sulfoxide (DMSO), used as solvent for rifampicin, bedaquiline and pretomanid. Crosses (x) indicate background level of luminescence. Black arrow indicates antibitotic addition. The experiment was performed in triplicate on two separate donors, and a representative experiment is shown. Statistical analyses were done using 2way ANOVA Tukey's multiple comparisons test; **** $p<0.0001$. The data are very consistent, so SEM bars are very narrow and obscured.

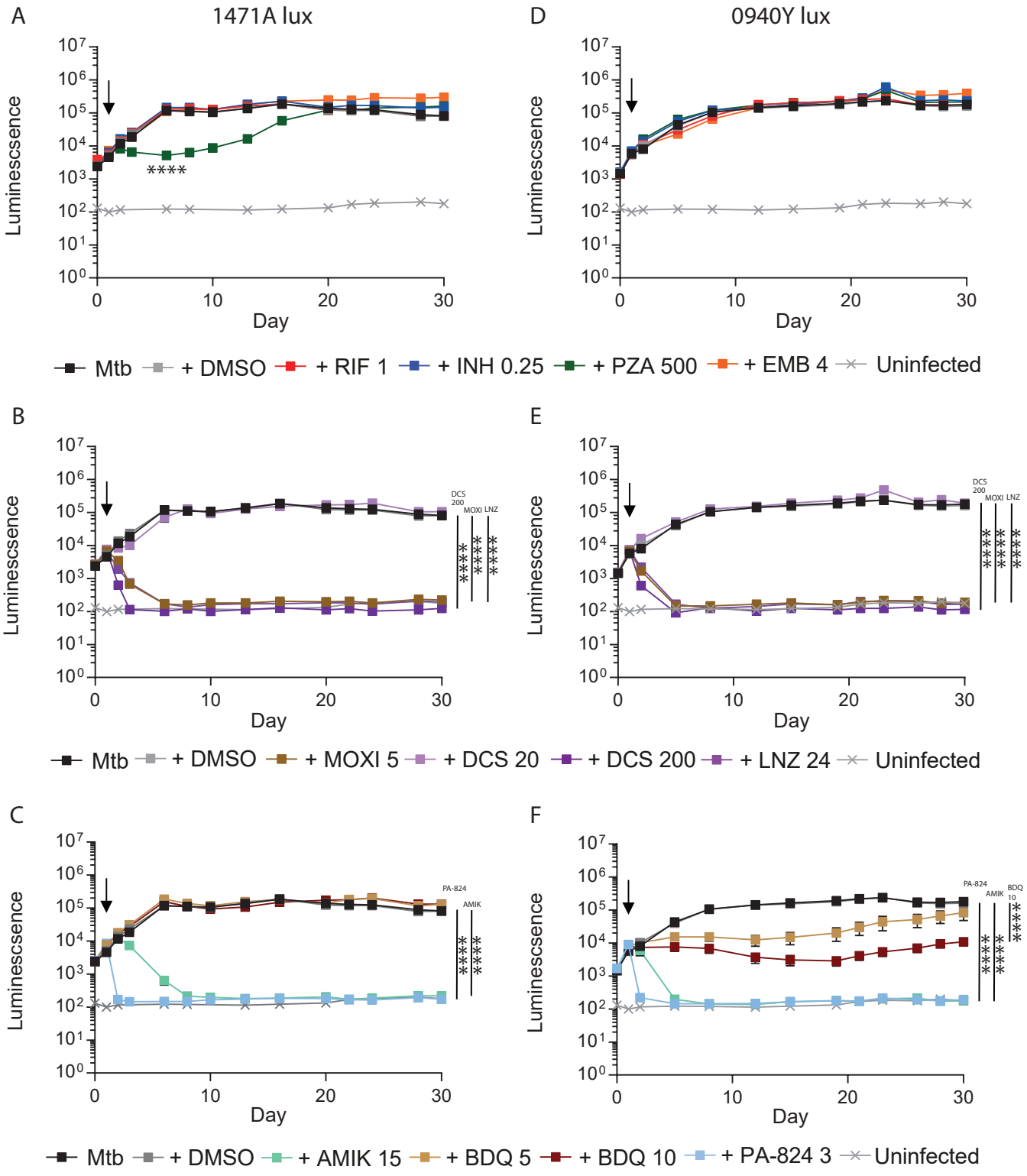

Fig. 5: Multi-drug resistant (MDR) strains demonstrate extensive antibiotic resistance. Antibiotics were added at day 1 to the 3-D model and Mtb growth monitored by luminescence; first-line drugs: rifampicin at 1µg/ml (RIF 1, dark red), isoniazid at 0.25µg/ml (INH 0.25, navy blue), pyrazinamide at 500µg/ml (PZA 500, dark green) and ethambutol at 4µg/ml (EMB 4, orange); second-line drugs: moxifloxacin at 5µg/ml (MOXI 5, light brown), D-cycloserine at 20µg/ml (DCS 20, lilac) and 200µg/ml (DCS 200, dark purple) and linezolid at 24µg/ml (LNZ 24, mid-purple); emerging drugs: bedaquiline at 5µg/ml (BDQ 5, beige) and 10µg/ml (BDQ 10, dark brown); and pretomanid at 3µg/ml (PA-824 3, light blue). 1471A lux strain confirmed resistance to rifampicin, isoniazid and ethambutol and showed partial sensitivity to pyrazinamide (A). Growth of this multi-drug resistant clinical isolate was unaffected by the lower concentration of D-cycloserine and bedaquiline (both concentrations tested) (B, C). 0940Y lux strain was resistant to all first-line antibiotics (D) and D-cycloserine at the lower concentration (E). 0940Y had partial sensitivity to bedaquiline (F). Bacteria were fully inhibited by all other antibiotics examined. Mtb growth was unaffected by addition of DMSO, used as solvent for rifampicin, linezolid, bedaquiline and PA-824. Crosses (x) indicate background level of luminescence. Black arrow indicates antibitotic addition. The experiment was performed in triplicate on two separate donors, and a representative experiment is shown. Statistical analyses were carried out using 2-way ANOVA with Tukey's multiple comparisons test; **** $p<0.0001$.

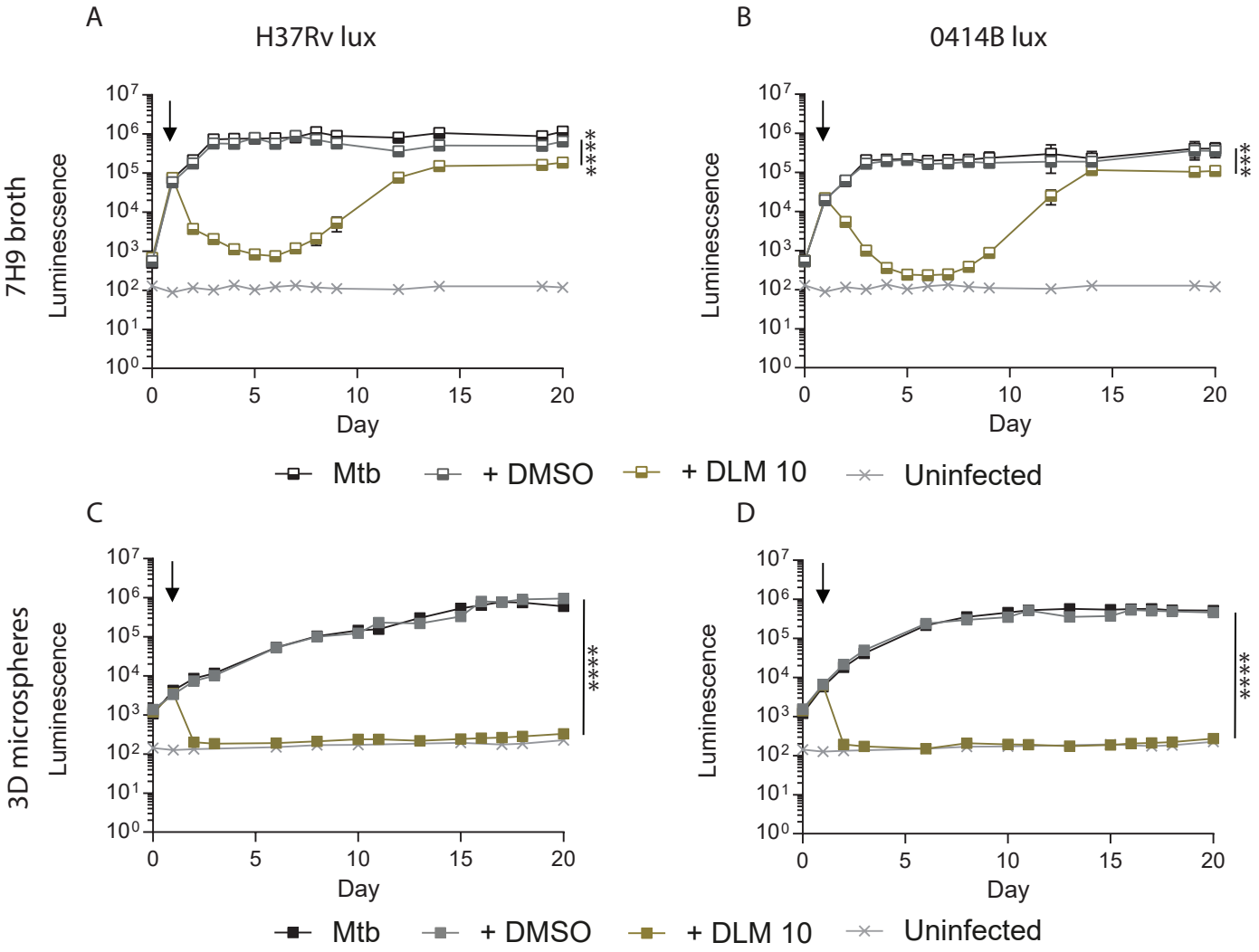

Fig. 6: Delamanid is more effective in microspheres than 7H9 broth. Delamanid was added at day 1 to either 7H9 broth (A, B) or infected microspheres (C, D) and Mtb growth monitored by luminescence. Bacteria were inhibited to the background level with delamanid at 10µg/ml (DLM 10, khaki green) in the microsphere system (C, D). Conversely, delamanid in 7H9 broth was much less effective in killing either H37Rv or O414B (A, B). Mtb growth was unaffected by DMSO, used as solvent for delamanid. Crosses (x) indicate background level of luminescence. Black arrow indicates antibiotic addition. The experiment was performed in triplicate on two separate donors, and a representative experiment is shown. Statistical analyses were performed using 2-way ANOVA with Tukey's multiple comparisons test; **** $p<0.0001$, *** $p<0.001$.

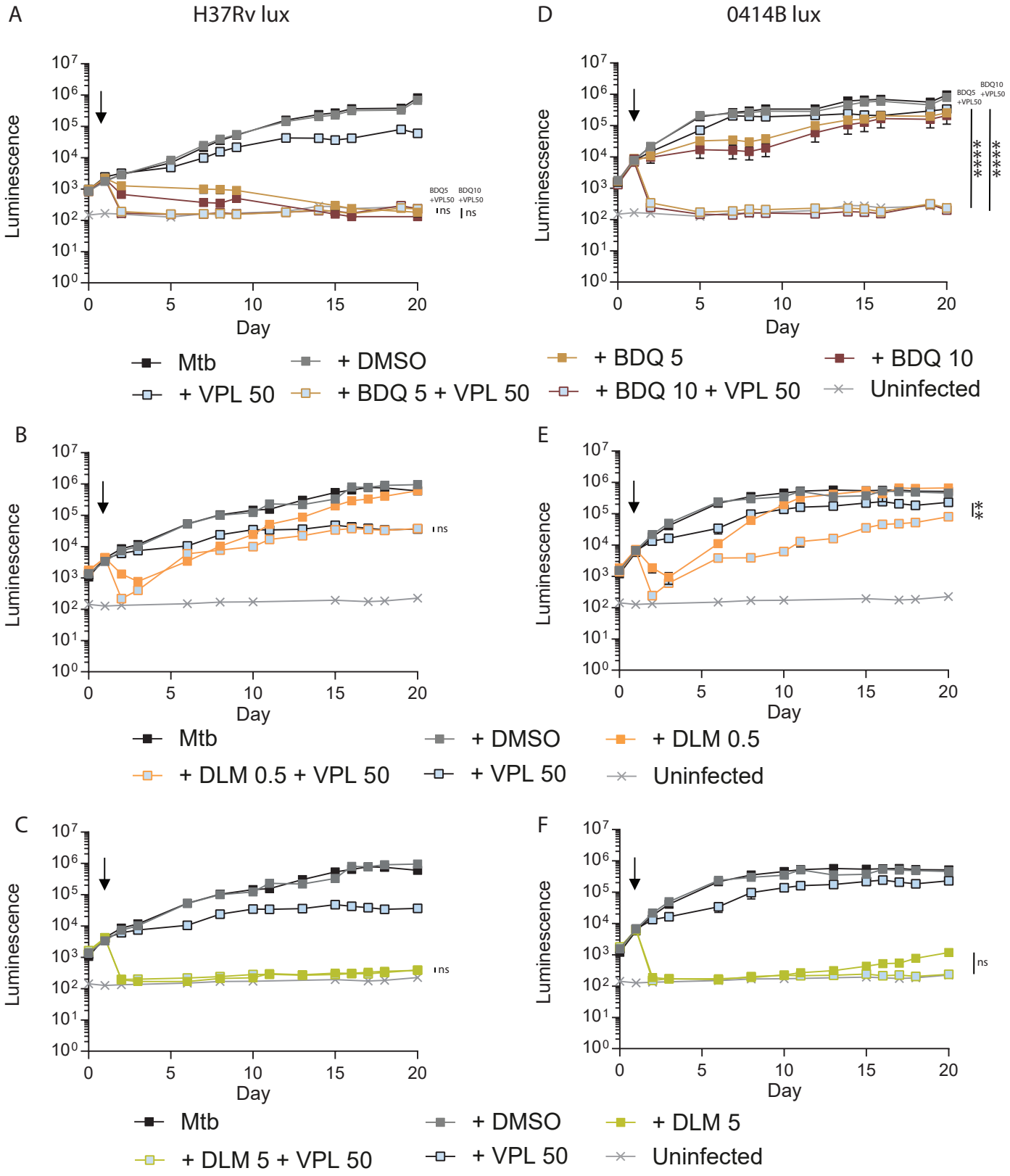

Fig. 7: Verapamil increases efficacy of bedaqualine and delamanid in 3-D culture. Compounds were added at day 1 to the microsphere system and Mtb growth monitored by luminescence; bedaquiline at 5µg/ml (BDQ 5, beige) and 10µg/ml (BDQ 10, dark brown); verapamil at 50µg/ml (VPL 50, light blue); delamanid at 0.5µg/ml (DLM 0.5, orange) and 5µg/ml (DLM 5, light green). Verapamil alone slightly reduced the growth of Mtb in all conditions. Verapamil potentiated the effect of bedaquiline for both H37Rv lux and 0414B lux in the 3-D system (A, D). Delamanid at 0.5µg/ml combined with verapamil had a greater killing effect on the clinical isolate than on H37Rv (B, E). Delamanid at the higher concentration inhibited the bacterial growth to the background level (C, F). Slight re-growth was observed at a later time point for 0414B lux, which was inhibited when combined with verapamil. Mtb growth was unaffected by DMSO, used as solvent for all the compounds tested. Crosses (x) indicate background level of luminescence. Black arrow indicates antibitotic addition. The experiment was performed in triplicate on two separate donors, and a representative experiment is shown. Statistics: 2way ANOVA Tukey's multiple comparisons test; **** $p<0.0001$, ** $p<0.01$, ns $p>0.05$

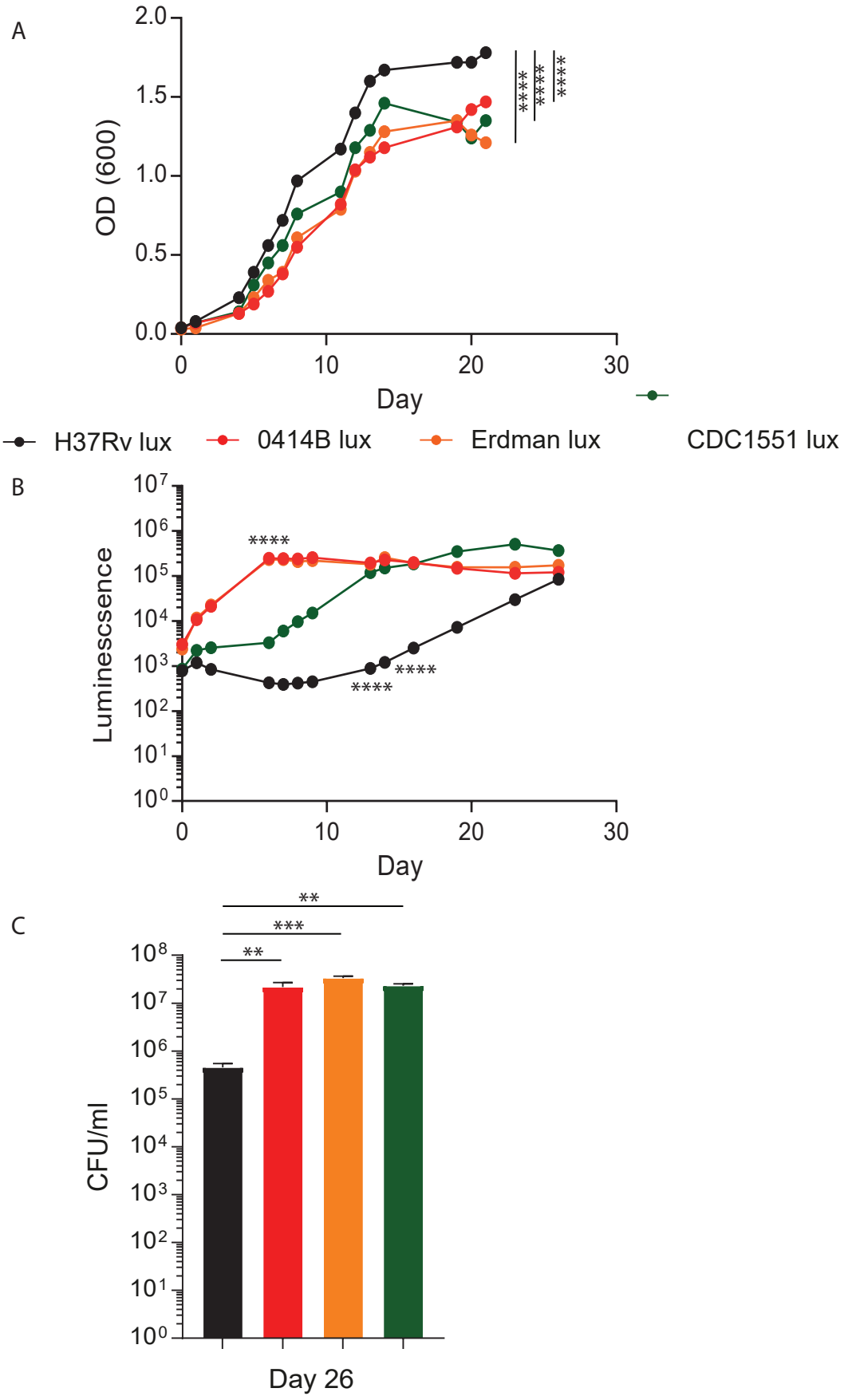

Fig. S1: Clinical isolate 0414B lux and other reference strains grow more rapidly in the 3-D model. (A) H37Rv lux grows faster than the clinical isolate 0414B lux and investigated reference strains (Erdman lux and CDC1551 lux) in Middlebrook 7H9 broth measured by optical density (OD) at 600nm. Experiments were performed in triplicate. **(B)** H37Rv lux is attenuated in comparison to the clinical isolate 0414B lux and the reference strains, Erdman lux and CDC1551 lux, in the 3-D system measured by luminescence. **(C)** Colony counts performed at day 26 confirm that H37Rv lux growth is reduced in comparison to the clinical isolate 0414B lux and the reference strains, Erdman lux and CDC1551 lux, in the 3-D system. Colour code as in (A) and (B). (B, C) Data are the mean ± the standard error of the mean of an experiment performed in triplicate and are representative of two separate experiments. Statistical analyses were carried out using 2-way ANOVA with Tukey's multiple comparisons test (A, B) or Ordinary one-way ANOVA Tukey's multiple comparisons test (C); **** $p<0.0001$, *** $p<0.001$, ** $p<0.01$.

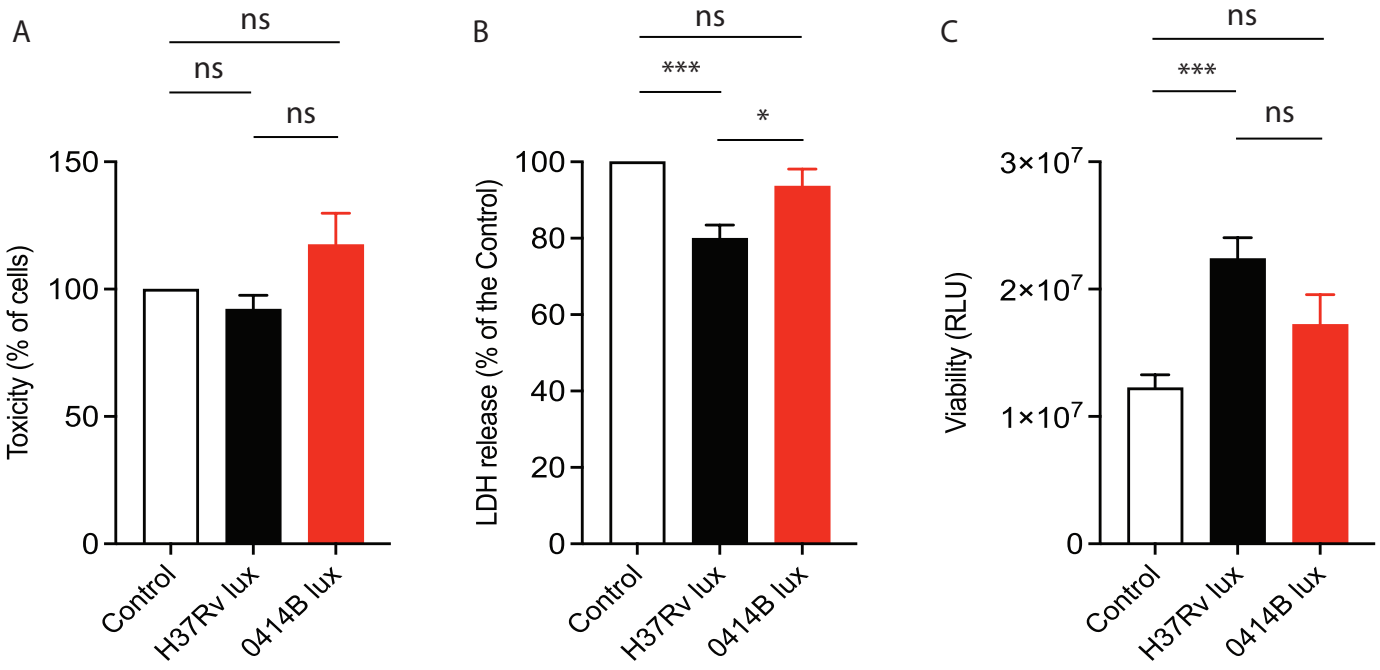

Fig. S2: Survival of host cells at day 7. Upon infection with either H37Rv lux (black), reduced cytotoxity compared to uninfected cells was noted by LDH release and Cell Titer-Glo 3-D cell viability assay. When compared to 0414B lux (red), no difference was observed in host cell toxicity measured by CytoTox-Glo cytotoxicity assay (A) or Cell Titer-Glo 3-D cell viability assay (C) between strains. Toxicity of host cells infected with H37Rv lux was significantly lower than cells infected with clinical isolate 0414B lux at day 7 when analysed by the LDH cytotoxicity assay (B). Data are mean +/- SEM of 3 separate experiments. Statistics: Ordinary one-way ANOVA with Tukey's multiple comparisons test (A,B,C); *** $p<0.001$, * $p<0.1$, ns $p>0.05$.

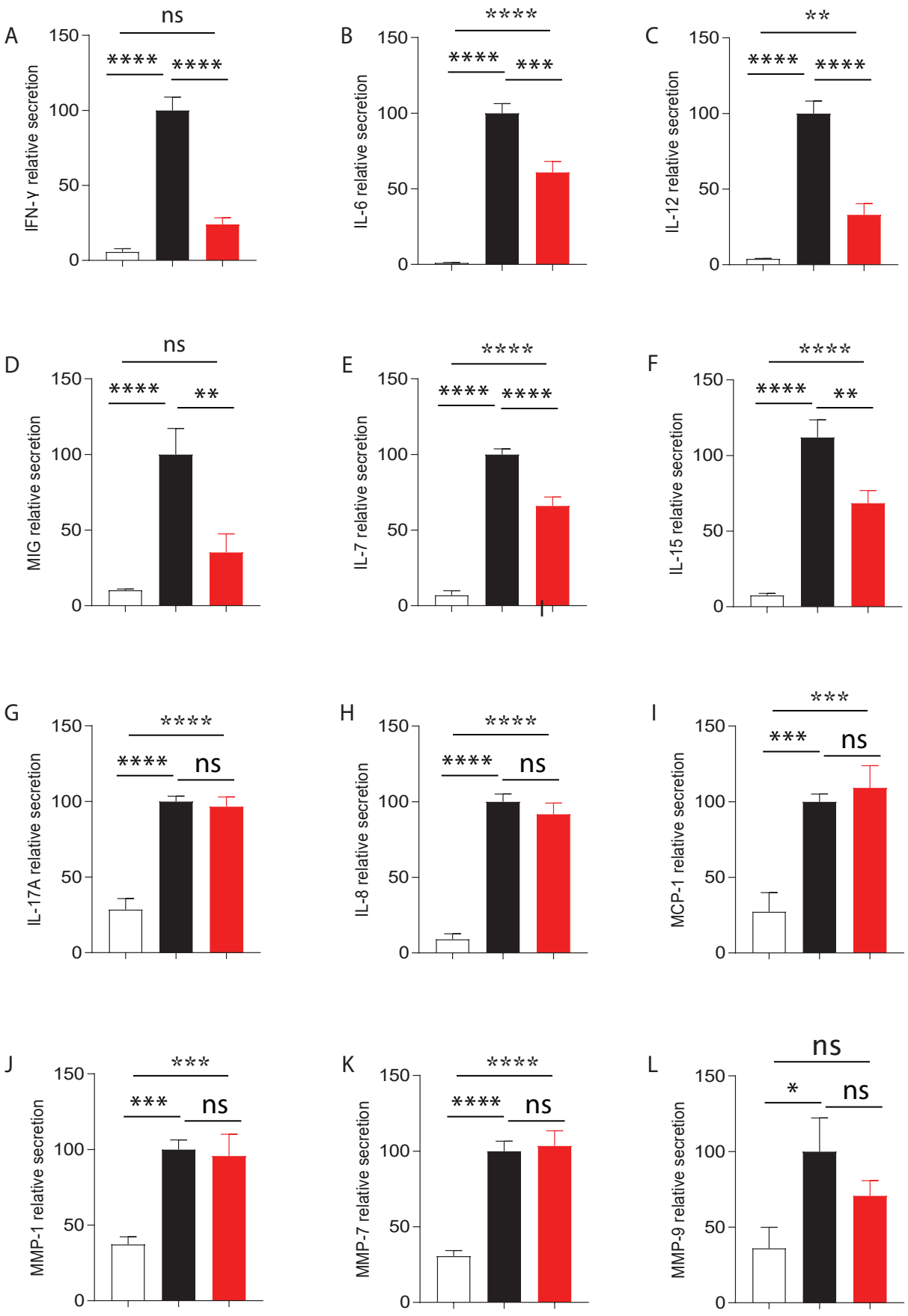

Fig. S3: Secretion of multiple cytokines by 0414B-infected cells is reduced relative to H37Rv infected cells. The clinical isolate 0414B lux was significantly less pro-inflammatory than the laboratory strain H37Rv lux. Panels A, B, C, D, E and F show six significantly different cytokines in response to the two strains. Panels G, H, I, J, K and L illustrate cytokines and MMPs that were secretion was similary upregulated in response to the two strains, analysed in the same samples by Luminex multiplex array. Uninfected PBMCs are control. Normalised data from two donors analysed in triplicate are presented (data are presented as a percentage vs H37Rv lux strain). Statistical analyses were performed using Ordinary one-way ANOVA with Tukey's multiple comparisons test; **** $p<0.0001$, *** $p<0.001$, ** $p<0.01$, * $p<0.1$, ns $p>0.05$.

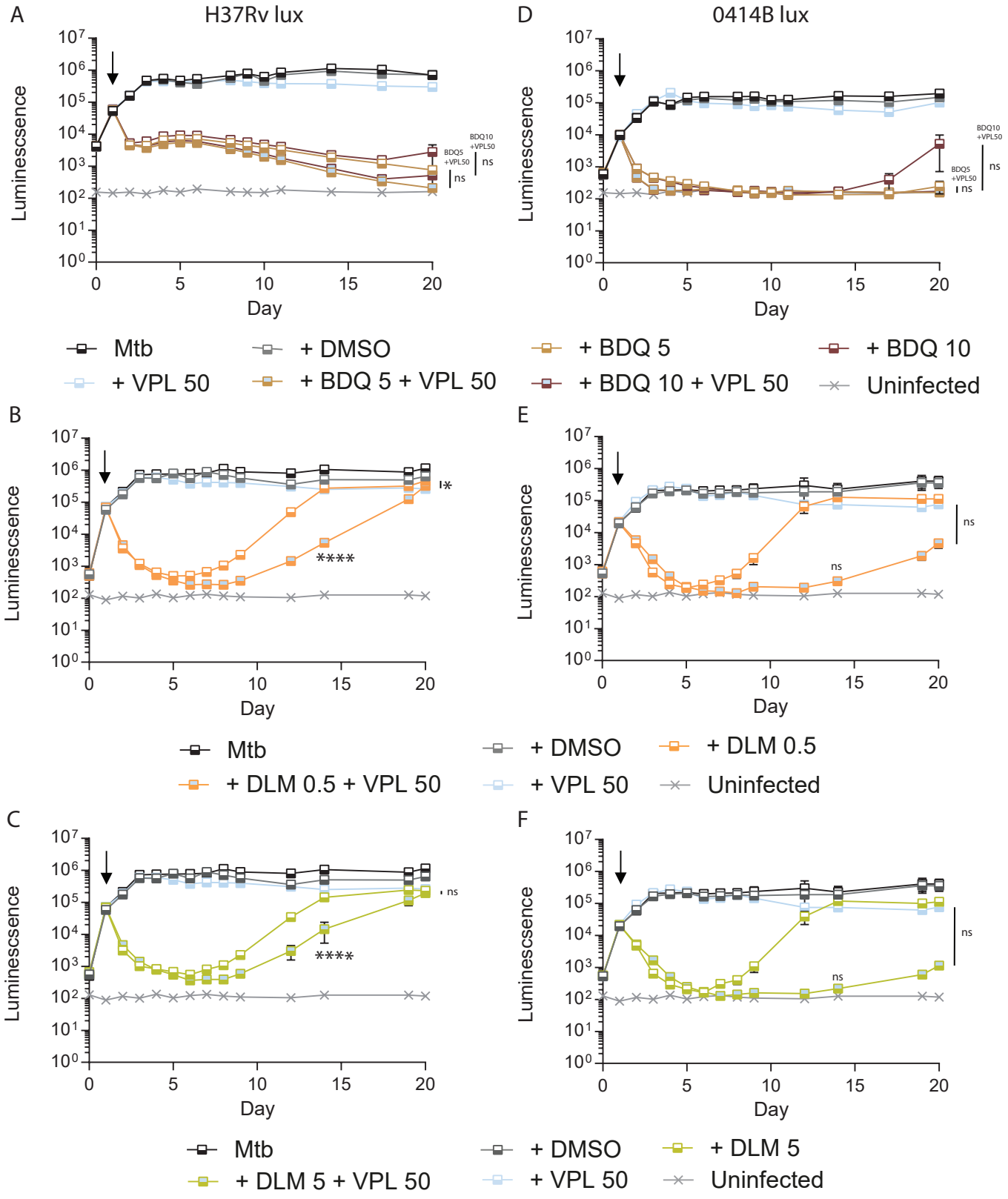

Fig. S4: Verapamil increases Mtb killing in 7H9 broth. Anti-TB drugs were added at day 1 to 7H9 broth and Mtb growth monitored by luminescence; bedaquiline at 5µg/ml (BDQ 5, beige) and 10µg/ml (BDQ 10, dark brown); verapamil at 50µg/ml (VPL 50, light blue); delamanid at 0.5µg/ml (DLM 0.5, orange) and 5µg/ml (DLM 5, light green). Verapamil alone did not affect initial growth of Mtb, and had a minimal inhibitory effect at later time points (A, B, C, D, E, F). Bedaquiline was more effective against the clinical isolate than the laboratory strain (A, B). Verapamil's potentiating effect on bedaquiline in killing bacteria was observed at later time points for H37Rv lux (A) and minimally 0414B lux (B). Delamanid had substantial killing effect on Mtb, however bacteria quickly recovered (B, C, E, F). The decrease in bacterial growth was potentiated by verapamil and it was considerably greater for the clinical isolate relative to H37Rv, but bacteria revived at later time points (B, C, E, F). Mtb growth was unaffected by DMSO, used as solvent for all the compounds tested. Crosses (x) indicate background level of luminescence. Black arrow indicates antibitotic addition. Data are mean +/- SEM for an experiment performed in triplicate and representative of 2 separate experiments. Statistical analyses were done using 2-way ANOVA with Tukey's multiple comparisons test; **** $p<0.0001$, * $p<0.1$, ns $p>0.05$.

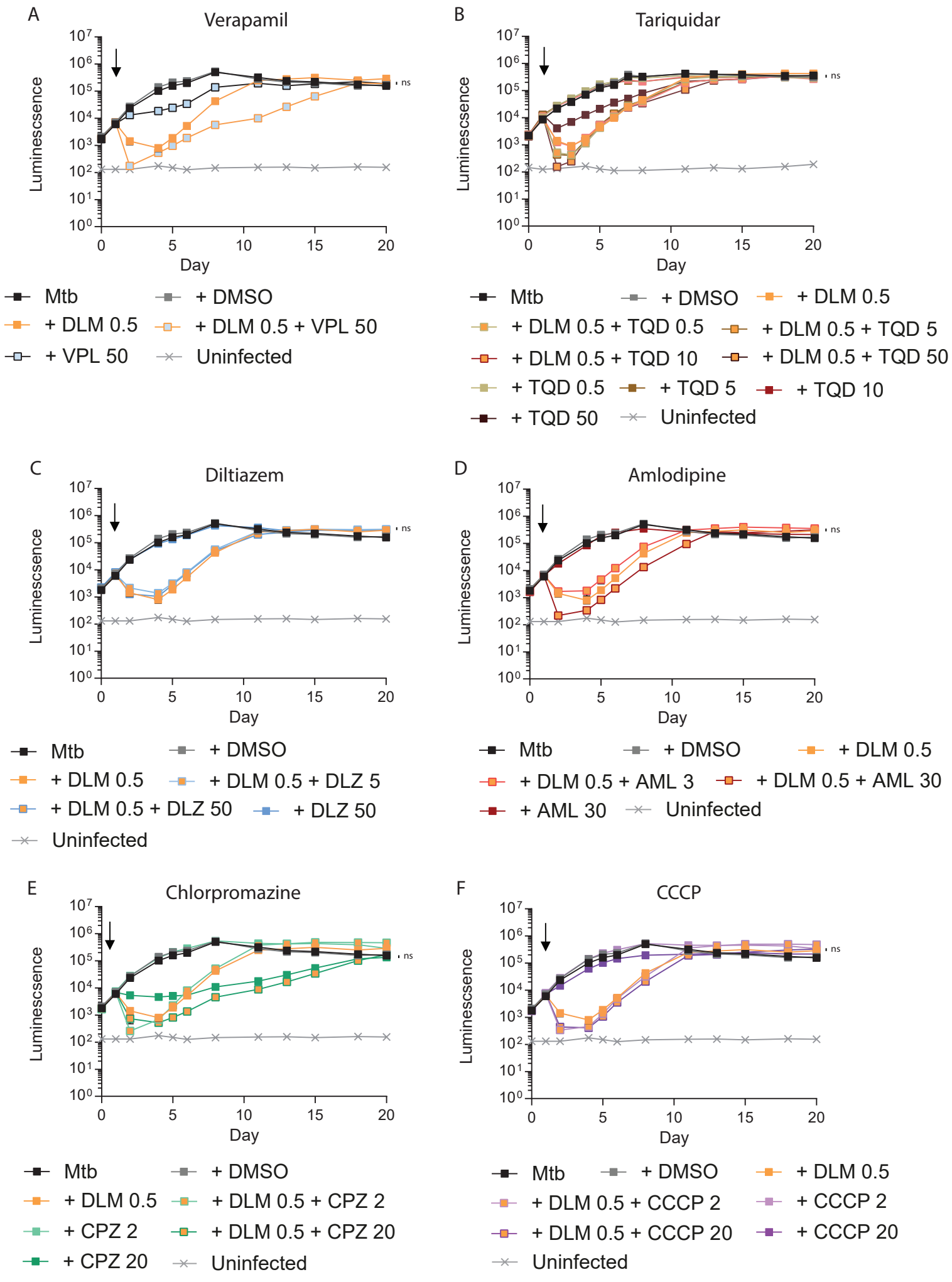
A
Verapamil
Luminescsence
Day
ns
Mtb
+ DMSO
+ DLM 0.5
+ DLM 0.5 + VPL 50
+ VPL 50
Uninfected
B
Tariquidar
Luminescsence
Day
ns
Mtb
+ DMSO
+ DLM 0.5
+ DLM 0.5 + TQD 0.5
+ DLM 0.5 + TQD 5
+ DLM 0.5 + TQD 10
+ DLM 0.5 + TQD 50
+ TQD 0.5
+ TQD 5
+ TQD 10
+ TQD 50
Uninfected
C
Diltiazem
Luminescsence
Day
ns
Mtb
+ DMSO
+ DLM 0.5
+ DLM 0.5 + DLZ 5
+ DLM 0.5 + DLZ 50
+ DLZ 50
Uninfected
D
Amlodipine
Luminescsence
Day
ns
Mtb
+ DMSO
+ DLM 0.5
+ DLM 0.5 + AML 3
+ DLM 0.5 + AML 30
+ AML 30
Uninfected
E
Chlorpromazine
Luminescsence
Day
ns
Mtb
+ DMSO
+ DLM 0.5
+ DLM 0.5 + CPZ 2
+ CPZ 2
+ DLM 0.5 + CPZ 20
+ CPZ 20
Uninfected
F
CCCP
Luminescsence
Day
ns
Mtb
+ DMSO
+ DLM 0.5
+ DLM 0.5 + CCCP 2
+ CCCP 2
+ DLM 0.5 + CCCP 20
+ CCCP 20
Uninfected

Figure S5

Fig. S5: Alternative efflux pump inhibitors combined with delamanid do not have as potent an effect as verapamil in the 3-D system. Compounds were added at day 1 to 3-D culture and Mtb growth monitored by luminescence; delamanid at 0.5µg/ml (DLM 0.5, orange); verapamil at 50µg/ml (VPL 50, light blue); tariquidar at 0.5µg/ml (TQD 0.5, light grey-green), 5µg/ml (TQD 5, light brown), 10µg/ml (TQD 10, dark red) and 50µg/ml (TQD 50, dark brown); diltiazem at 5µg/ml (DLZ 5, light blue) and 50µg/ml (DLZ 50, mid-blue); amlodipine at 3µg/ml (AML 3, bright red) and 30µg/ml (AML 30, dark red); chlorpromazine at 2µg/ml (CPZ 2, light green) and 20µg/ml (CPZ 20, dark green); carbonyl cyanide 3-chlorophenylhydrazone at 2µg/ml (CCCP 2, lilac) and 20µg/ml (CCCP 20, mid-purple). Verapamil showed a potentiating effect on delamanid in inhibiting Mtb growth (A). Addition of tariquidar, diltiazem or CCCP to delamanid had no effect at the concentrations tested (B, C, F). Supplementation of amlodipine with delamanid had minimal effect but only at a higher concentration used (D). Similarly, combining chlorpromazine 20µg/ml with delamanid showed very slight Mtb killing effect (E). Higher concentrations of tariquidar and chlorpromazine applied on their own (50µg/ml and 20µg/ml, respectively) had some inhibitory effect on the clinical isolate (B, E). Mtb growth was unaffected by DMSO, used as solvent for all the compounds tested. Crosses (x) indicate background level of luminescence. Black arrow indicates antibitotic addition. Data are mean +/- SEM for an experiment performed in triplicate and representative of 2 separate experiments. Statistical analyses were carried out using 2-way ANOVA with Tukey's multiple comparisons test; ns $p>0.05$